Timing of granulite-facies metamorphism in the eastern Himalayan syntaxis and its tectonic implications

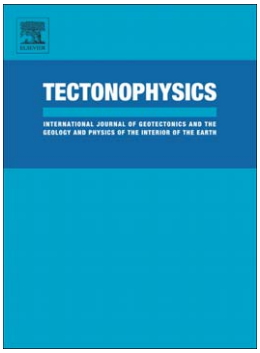

Timing of granulite-facies metamorphism in the eastern Himalayan syntaxis and its tectonic implications

Wang-Chun Xu, Hong-Fei Zhang, Randall Parrish, Nigel Harris, Liang Guo, Hong-Lin Yuan

PII: S0040-1951(10)00002-8
DOI: doi: 10.1016/j.tecto.2009.12.023
Reference: TECTO 124830

To appear in: *Tectonophysics*

Received date: 7 May 2009
Revised date: 24 October 2009
Accepted date: 30 December 2009

Please cite this article as: Xu, Wang-Chun, Zhang, Hong-Fei, Parrish, Randall, Harris, Nigel, Guo, Liang, Yuan, Hong-Lin, Timing of granulite-facies metamorphism in the eastern Himalayan syntaxis and its tectonic implications, *Tectonophysics* (2010), doi: 10.1016/j.tecto.2009.12.023

Timing of granulite-facies metamorphism in the eastern Himalayan syntaxis and its tectonic implications

Wang-Chun Xu[a], Hong-Fei Zhang[a*], Randall Parrish[b], Nigel Harris[c], Liang Guo[a], Hong-Lin Yuan[d]

[a] *State Key Laboratory of Geological Process and Mineral Resources, China University of Geosciences, Wuhan 430074, P.R. China*

[b] *Department of Geology University of Leicester and NERC Isotope Geosciences Laboratory, British Geological Survey, Keyworth, Notts NG12 5GG, UK*

[c] *Department of Earth Sciences, The Open University, Milton Keynes, MK7 6AA,UK*

[d] *State Key Laboratory of Continental Dynamics, Northwest University, Xi'an, 710069, P.R. China*

A revised manuscript submitting to Tectonophysics for review

[*] Corresponding author. e-mail: hfzhang@cug.edu.cn

Abstract

We present geochronological evidence in the eastern Himalayan syntaxis (Namche Barwa) for high-pressure (HP) granulite-facies metamorphism and explain its importance for understanding both the deep continental subduction of the Indian plate beneath Asia and its subsequent exhumation. The timing of peak and retrograde metamorphism in part constrains these processes but is debated. We present zircon U-Pb and trace element data on granulite-facies rocks. Zircon cores and rims from a weakly retrograded mafic granulite (P=14-18 kbar, T≈800 ℃) yield U-Pb ages of 24.0±0.3 Ma and 18.8±0.3 Ma, respectively. Zircon cores and rims from an orthogneiss, the host of the mafic granulite, yield U-Pb ages of 490±3 Ma and 24.2±0.4 Ma, respectively. An amphibolitized mafic granulite gives a U-Pb zircon age of 17.0±0.4 Ma. Combined with petrography, zircon CL images, Th/U ratios and REE patterns, we suggest that the peak metamorphic age for the HP granulite is at ~24 Ma and subsequent moderate- and low-pressure retrograde metamorphism occurred at 19-17 Ma, indicating reasonably rapid exhumation for the HP granulite. The ages of detrital zircons from a metasedimentary rock, another host rock of the mafic granulite, range from ~0.6 to ~2.0 Ga with peak at 0.8-1.2 Ga. The protolith depositional ages for the metasedimentary rock are constrainted to be between 490 and ~600 Ma. Our data suggest that the granulite terrane in the eastern Himalayan syntaxis has an affinity with the Greater Himalayan Series. The HP granulite-facies metamorphic events in the eastern Himalayan syntaxis are distinct from ultra-high pressure (UHP) metamorphic events in the western Himalayan syntaxis in both age and depth of burial. However, the metamorphic history of the eastern and western Himalayan syntaxises becomes similar after ~24 Ma. The Namche Barwa granulites appear to result from the underthrusting of the Indian plate lithologies beneath the Lhasa block during progressive collisional processes, followed by extrusion and/or exhumation that result from a slab breakoff of the Indian plate during the Miocene.

Keywords: U-Pb zircon dating, trace element, high-pressure granulite, Namche Barwa group, eastern Himalayan syntaxis

1. Introduction

The 2500 km long, east-west-trending Himalaya is the most promising orogen on the Earth to study continent-continent collision processes (e.g., Argand 1924; Gansser, 1964; Hodges, 2000; Yin, 2006). Exposures of high-pressure (HP) metamorphic rocks within the Himalayan orogen provide particular insights about the collisional and exhumation process (Tonarini et al., 1993; Guillot et al., 1997; Ding et al., 2001). In the western Himalayan syntaxis, the coesite-bearing ultrahigh-pressure (UHP) eclogites, occurring in the Tso Morari and Kaghan areas, have demonstrated that the continental crust of the entire northwestern part of the Indian plate was subducted beneath the Kohistan-Ladakh arc to a minimum depth of 90 km (O'Brien et al., 2001; Mukherjee and Sachan, 2003). Chronologic investigations show that the UHP metamorphism occurred in the Early Eocene (de Sigoyer et al., 2000; Kaneko et al., 2003; Leech et al., 2005; Parrish et al., 2006). In the eastern Himalayan syntaxis, the eastern termination of the Himalayan orogen, HP granulites are present but no eclogite has yet been recorded (Zhong and Ding 1996; Liu and Zhong, 1997). Chronological study of the granulite-facies metamorphism, however, has yielded contentious results (Ding and Zhong, 1999; Ding et al., 2001; Liu et al., 2007). Early zircon U-Pb and clinopyroxene Ar-Ar dating suggested granulite-facies peak metamorphism occurred between 69 Ma and 45 Ma, and retrograde metamorphism between 23 Ma and 18 Ma (Ding and Zhong, 1999). Recently, using the U-Pb zircon dating method, Ding et al. (2001) obtained two groups of metamorphic ages for mafic granulite samples: ~40 Ma and 11-25 Ma. They interpreted the ca.40 and ca.11 Ma ages to represent the timing of HP and moderate-pressure (MP) metamorphism, respectively. The ages between 11 and 25 Ma were interpreted as mixing with an older component though the

lack of analyses of crystal zoning renders this interpretation speculative. Liu et al. (2007) carried out U-Pb zircon dating of a garnet-sillimanite gneiss, the host rock of the mafic granulite. They obtained ages of ca.500 Ma for zircon cores while zircon rims yielded two groups of ages: 30-33 Ma and ~23 Ma. The first group was interpreted as HP peak metamorphic age and the second group was interpreted as HP retrograde metamorphic age. Together these data remain contradictory and with a lack of stronger supporting data, the age of both HP and retrogressive metamorphism remains unclear.

U-Pb zircon dating, combined with zircon trace element analyses can provide powerful constraints on zircon growth and zircon age interpretation (e.g., Hermann et al., 2001; Rubatto, 2002; Whitehouse and Platt, 2003; Bingen et al., 2004; Tomkins et al., 2005). In this paper, we present LA-ICP-MS microprobe U-Pb zircon data, coupled with zircon trace element analyses, from two mafic granulites, a host orthogneiss and a high-grade metasedimentary rock in the eastern Himalayan syntaxis. We use these data to discuss the timing of the peak and retrograde metamorphism for the granulites, the tectonic position of the HP granulite terrane and tectonic evolution in the eastern Himalayan syntaxis in an attempt to resolve this controversy.

2. Geologic setting

2.1 Regional geology

The eastern Himalayan syntaxis (EHS) (Fig.1) is the eastern termination of the Himalaya collisional orogen. The main structural features of the Himalaya and the primary geological unit subdivisions bend strongly around an uplifted area at Namche Barwa and coincide with the ‘U-turn’ of the Yalu-Tsangpo River (Burg et al., 1998; Zeitler et al., 2001). The EHS comprises three major tectono-stratigraphic units (Geng et al., 2006): (1) the Namche Barwa group of high grade metamorphic rocks; (2) the Indus-Yarlung suture (IYS);

(3) the Gangdese magmatic belt. The northwestern and southeastern contacts between the Namche Barwa group and the Gangdese magmatic belt are the sinistral Dongjiu-Miling fault and dextral Aniqiao fault, respectively. The syntaxis is cut at its northeastern tip by the active dextral Jiali-Parlung fault (Burg et al. 1997, 1998; Zhang et al., 2004).

The Namche Barwa Group, the core of the EHS, is dominantly layered quartz-feldspar-biotite gneiss with a migmatitic character (Burg et al., 1998). According to recent geological mapping (Geng et al., 2006), it can be subdivided into three mappable lithological subunits: Zhibai formation, Duoxiongla migmatite and Paixiang formation (Fig.1). The Zhibai formation is the most highly metamorphosed and has undergone high-temperature ductile deformation. It comprises garnet-bearing gneiss with sporadic boudins of mafic granulite (garnet clinopyroxenite), kyanite granulite and garnet amphibolite (Fig.2; Liu and Zhong, 1997; Geng et al., 2006). The Duoxiongla migmatite is composed of migmatitic gneiss and orthogneiss with protolith ages ranging from 1.6 Ga to 1.8 Ga by U-Pb zircon dating (Guo et al., 2008). The Paixiang formation is dominantly felsic gneiss with subordinate diopside and forsterite-bearing marble, clinopyroxenite and scapolite diopsidite (Geng et al., 2006). The Namche Barwa Group is intruded by young granitoids with ages of 3-13 Ma (Burg et al., 1998; Ding et al., 2001; Booth et al., 2004).

The IYS unit is the middle tectonic unit separating the Namche Barwa group in the Indian plate from the Gangdese magmatic belt in the Asian plate (Fig.1). It is a 2-10 km wide continuous zone, consisting of highly deformed metasedimentary and ultramafic-mafic rocks, the latter representing slices of the Neo-Tethyan oceanic slab (Geng et al., 2006). The geochemical data on the IYS dismembered mafic volcanic rocks show a back-arc basin affinity, which is comparable to those of the IYS suture zone at Xigatze and Zedang (Geng et al., 2006). Clinopyroxene $^{40}Ar/^{39}Ar$ dating study suggested the crystallization age at 200±4 Ma for the IYS ophiolite (Geng et al., 2004).

The Gangdese magmatic belt lies to the west, north and east of IYS (Fig.1). It is mainly composed of the Nyingchi group and intrusive granites. The Nyingchi group has been divided into lower, middle, and upper parts (YIGS, 2005). The lower Nyingchi group comprises amphibolitic gneiss and leptynite intercalated with mafic granulite; the middle Nyingchi group consists of biotite paragneiss and granitic gneiss intercalated with kyanite-sillimanite biotite schist and marble; the upper Nyingchi group consists of kyanite-sillimanite-garnet two-mica schist and biotite schist intercalated with biotite gneiss, marble, and leptynite. Detrital zircon age data suggest that the maximum depositional age of the middle-upper Nyingchi group is less than 60 Ma, and the maximum depositional age of the lower Nyingchi group is no older than 490 Ma (Zhang et al., 2008). The Gangdese granites in the eastern Himalayan syntaxis were mostly emplaced during two episodes of ~133-110 Ma and ~66-57 Ma (Booth et al., 2004, 2009; Chiu et al., 2009). The Early Cretaceous granites were probably generated in a post-collisional regime in response to the Late Jurassic-Early Cretaceous collision between the Qiangtang and Lhasa terranes (Chiu et al., 2009). The Late Cretaceous-Paleocene granites resulted from northward Neotethyan subduction during late Mesozoic time (Chiu et al., 2009). They are intruded by the later muscovite granite, two-mica granite and garnet granite, ranging from 26 Ma to 21 Ma in age (Ding et al., 2001; Chung et al., 2003; Booth et al., 2004; Zhang et al., 2008). They could be related to the Gangdese thrust event (Booth et al., 2004) or the removal of the tectonically thickened lithospheric mantle in the late Oligocene time (Chung et al., 2003).

2.2 P-T conditions for the Zhibai formation

For the granulite-bearing complex (Zhibai formation), early work has shown that two metamorphically distinct mineral assemblages occur in the pelitic gneiss (Liu and Zhong, 1997). The peak metamorphic assemblage is garnet+kyanite+rutile+feldspar+quartz. They

were formed at P≈14-18 kbar and T≈850 ℃ (Liu and Zhong, 1997; Ding et al., 1999), estimated by a Grt-Ky-Qz-An (GASP) barometer (Newton and Haselton, 1981) and coupled with a two-feldspar thermometer (Kroll et al., 1993) as well as a Grt-Bi (GARB) thermometer (Berman, 1990). The P-T estimates are supported by Booth et al. (2009), using THERMOCALC. Exhumation of the gneisses produced low-pressure assemblages marked by cordierite+spinel at P≈5 kbar and T≈850 ℃ (Liu and Zhong., 1997; Ding et al., 1999), estimated by a Grt-Bi thermobarometer (New and Haselton, 1981; Hodges and Spear, 1982) and a Crd+Sil+Grt+Qz (CAGS) thermobarometer (Wells, 1979). Boudins of mafic granulite are common in these gneisses. These rocks are composed of nearly equal garnet and pyroxene. In field exposures, the retrograded garnet-amphibolite and amphibolite usually occur on the outer margins of the mafic granulite (Zhong and Ding, 1996; Zhang et al., 2007). On the basis of microstructural observations and mineral relationships, three metamorphic stages and related mineral assemblages have been recognized by Zhong and Ding (1996): (1) M1-HP granulite-facies assemblages, consisting of garnet, clinopyroxene and minor quartz; (2) M2-MP granulite-facies assemblages, characterized by the symplectite of plagioclase+orthopyroxene+clinopyroxene after garnet; (3) M3, amphibolite-facies assemblages, including hornblende+plagioclase+biotite. According to thermometer by Ellis and Green (1979), the peak temperature is ~800 ℃ (Zhong and Ding, 1996). Referring to reaction Opx+An=Grt+Qz described by Zhai et al. (1992), Zhong and Ding (1996) argued that the peak pressure is 14-15 kbar corresponding to 800 ℃. This is consistent with the above pelitic gneisses (Liu and Zhong, 1997; Ding et al., 1999). The MP metamorphic conditions for the M2 assemblages were defined by Zhong and Ding (1996) at P=8~10 kbar and T=800~900 ℃ (Opx-Cpx thermobarometer, Wood and Banno, 1973; Harley, 1984). According to the Am-Pl thermobarometer by Perchuk (1966) and Plyusnina (1982), the amphibolite-facies assemblages (M3) formed at P=4.5~6 kbar and T=650~700 ℃ (Zhong and

171Ding 1996), which is also consistent with that of the above pelitic gneisses. Together, the 172thermobarometric studies on both the pelitic gneisses and mafic granulites from Namche 173Barwa yield similar steep clockwise P-T paths (Fig.3).

174

175**2.3 Sample description**

176 Four samples were selected for geochronological analysis (Fig. 1). These samples were 177collected from the granulites-bearing complex in the Zhibai formation (GPS: N 29°38′18.7″; 178E 94°56′57.9″). Two mafic granulite samples (T605 and T604) were colleted in a boudin of 179mafic lithologies. While the sample T604 from the margin of the boudin, the sample T605 180collected from the core of the boudin. Sample T605 is a weakly retrograded mafic granulite, 181consisting mainly of amphibole (~50%), clinopyroxene (17%), plagioclase (~18%), garnet 182(~10%), quartz (~3%), ilmenite (~1%) and titanite (~1%) (Fig.4a). Thin-section observation 183shows garnet breakdown to amphibole-plagioclase, locally to clinopyroxene-plagioclase 184symplectite. These retrograded minerals are preserved in the narrow coronas rimming garnet 185with grain size of 30-100 μm and vermiform and embayed outline (Fig.4a). The retrogression 186of sample T604 is much stronger than for the sample T605. It is a completely amphibolitized 187granulite containing the assemblage amphibole (~67%), plagioclase (~30%) and biotite (~3%) 188(Fig.4b). Besides, two gneiss samples (T602 and T609) were collected from the host rocks of 189the mafic granulites. Sample T609 is a garnet-bearing granitic gneiss. It consists of quartz 190(~25%), K-feldspar (~35%), plagioclase (~25%), biotite (~10%) and garnet (~5%) (Fig.4c). 191Sample T602 is a pelitic gneiss. It consists of quartz (~30%), plagioclase (~30%), K-feldspar 192(~10%), biotite (~20%) and garnet (~10%) (Fig.4d).

193

194**3. Analytical methods**

195 Zircons were separated from rock samples using conventional techniques. The zircon

crystals were mounted in an epoxy disc and then were polished to expose internal sections. Cathodoluminescence (CL) imaging for the zircons was carried out at the State Key Laboratory of Continental Dynamics, Northwest University, Xi'an, China. Using CL images to differentiate growth zoning and core-rim positions, the zircons were analyzed for U-Th-Pb isotopic compositions and U, Th, Pb and REE concentrations using LA-ICP-MS methods at the State Key Laboratory of Geological Process and Mineral Resources, China University of Geosciences, Wuhan, China. The laser spot was 32 μm in diameter with He as transport gas. Measurements were corrected using calibration to reference zircon standard 91500 and NIST SRM 610 glass. The detailed analytical procedures are similar to those reported in Yuan et al. (2004). The common Pb correction use the EXCEL program of ComPbCorr#3-151 (Andersen, 2002), assuming that the observed $^{206}Pb/^{238}U$, $^{207}Pb/^{235}U$ and $^{208}Pb/^{232}Th$ ratios for a discordant zircon can be accounted for by a combination of lead loss at a defined time. Data processing is carried out using Isoplot (Ludwig, 2003).

4. Results

4.1 Sample T605

Zircons in T605 are colourless and anhedral. They are oval to round crystals, and have grain sizes of 50-150 μm in length, with ratios of length to width ranging from 1:1 to 2:1. CL images reveal that most grains comprise a core, surrounded by a weakly luminescent rim (Fig.5a). The core and rim exhibit weak planar zoning or no zoning. The boundary between the core and rim is rounded, straight or embayed, suggesting possible resorption and recrystallization. In addition, the sample contains rounded grains up to 150 μm in diameter, which are similar to the weak luminescent rims in CL images, suggesting that nucleation of new zircon is coeval with the CL-dark zircon rims. These grains make up around 10% of the total zircon population. They will be discussed together with the zircon rims. Both the zircon

221morphology and internal structure indicate that they are metamorphic in origin (Vavra et al., 2221996, 1999; Corfu et al., 2003).

223 Twenty-three core analyses (Table 1) show $^{206}Pb/^{238}U$ ages that cluster about a weighted 224mean $^{206}Pb/^{238}U$ age of 24.0±0.3 Ma (2σ; MSWD=0.69), with two additional cores slightly 225older at ca.30 Ma (Fig.6a). Eight rim analyses define a cluster of $^{206}Pb/^{238}U$ ages with a 226weighted mean $^{206}Pb/^{238}U$ age of 18.8±0.3 Ma (2σ; MSWD=0.55; Fig.6a). The cores have U of 22799~490 ppm, Th of 2.6~37.5 ppm and Th/U ratios of 0.02~0.08. The rims display higher U 228(1202~2112 ppm) and Th (42~98 ppm) than the cores, but their Th/U ratios (0.03-0.05) are 229not distinct from the cores (Fig.7). The low Th/U ratios for the cores and rims are consistent 230with a metamorphic origin (Rubatto, 2002), which is also consistent with the CL images. The 231total REE contents of the cores and rims (Table 2) range from 12.2 to 114.3 ppm and from 23242.5 to 88.2 ppm, respectively. The cores have slightly steep chondrite-normalized MREE-233HREE patterns ($(Yb/Gd)_N$=3.4~15.4) with pronounced positive Ce anomalies (Ce/Ce*=9~67) 234and weakly negative or positive Eu anomalies (Eu/Eu*=0.56~1.16, cluster around 0.92) 235(Fig.8a). There is, however, a marked difference in REE composition between the rims and 236cores. The rims have apparent negative Eu anomalies (Eu/Eu*=0.39-0.54) and higher MREE 237contents, resulting in more flat chondrite-normalised MREE-HREE patterns ($(Yb/Gd)_N$=1.2-2385.3)) (Fig.8b).

239

240**4.2 Sample T604**

241 Most zircons from T604 are short to long prismatic crystals, but generally have rounded 242terminations. They have grain sizes of 100~400 μm in length, with ratios of length to width 243ranging from 1:1 to 3:1. In CL images (Fig.5b), most zircons show weakly planar or sector 244zones, which are typically metamorphic (Vavra et al., 1996, 1999; Corfu et al., 2003).

245 All twenty-two analyses on fifteen zircon grains yield $^{206}Pb/^{238}U$ ages between 15.7±0.8

246and 18.0±1.0 Ma (Table 1), with a weighted mean of 17.0±0.4 Ma (2σ; MSWD=0.96) 247(Fig.6b). The zircons have U of 67.4~ 448.4 ppm, Th of 4.7~29.6 ppm and Th/U ratios of 2480.03~0.10 (Fig.7). The total REE contents of these zircons range from 88.7 to 317.3 ppm. 249They have steep chondrite-normalized MREE-HREE patterns ($(Yb/Gd)_N$=47-77) with both 250pronounced positive Ce anomalies (Ce/Ce*=19-72) and negative Eu anomalies 251(Eu/Eu*=0.32-0.89; Fig.8c). The zircons from T604 show strikingly elevated HREE contents 252and much steeper REE patterns than the zircon cores and rims from T605 (Fig.8).

253

254**4.3 Sample T609**

255 Zircons from T609 are long prismatic with an aspect ratio of ca. 4:1. Their CL images 256(Fig.5c) exhibit complicated core and rim structures. Rounded cores are rarely present. More 257common are angular cores with oscillatory zoning and forms of resorption, interpreted as 258inherited magmatic zircons (Corfu et al., 2003). The non-luminescent rims are weakly zoned 259or not zoned, implying that they are metamorphic (Vavra et al., 1996, 1999; Corfu et al., 2602003). The contacts between the luminescent cores and the non-luminescent rims are angular, 261sharp, and cut across the zonation patterns in the cores (Fig.5c).

262 Twelve zircon rims were dated (Table 1). Among them, one analysis (Th/U=0.05) has a 263$^{206}Pb/^{238}U$ age of 17±0.5 Ma, and the remaining eleven analyses (Th/U=0.01 to 0.05) yield a 264cluster of $^{206}Pb/^{238}U$ ages with a weighted mean $^{206}Pb/^{238}U$ age of 24.2±0.4 Ma (2σ; 265MSWD=0.74; Fig.6d). Twenty-two analyses on oscillatory zoning cores (Th/U=0.22-0.60) 266form a coherent group with a weighted mean $^{206}Pb/^{238}U$ age of 490±3 Ma (MSWD=0.17) 267(Fig.6c). Two analyses on round cores (Th/U=0.34~0.56) have $^{207}Pb/^{206}Pb$ ages of 821±20 and 2681225±66 Ma (Table 1). It would appear that the protolith of this granitic gneiss was 490 Ma 269old with a small amount of older inheritance, and that it was metamorphosed to create rims 270during events mainly at 24 Ma but extending to as young as 17 Ma.

271

272**4.4 Sample T602**

273 Zircons from T602 are characterized by round, sub-round and irregular crystals, 274indicating that they are detrital (Davis 2002). CL images reveal that most grains comprise a 275core, surrounded by a weak luminescent rim (Fig.5d). Most zircon cores exhibit clear 276resorption structures. The contacts between the cores and rims are angular or embayed, 277indicating the zircon rims have been produced by recrystallization.

278 Twenty-five zircon cores were dated (Table 1). They are concordant and near-279concordant, and yield $^{207}Pb/^{206}Pb$ ages of ~600 to ~2000 Ma with peak at 800-1200 Ma (Fig.6e 280and f). The cores have U of 111~2329 ppm, Th of 49.3~550.2 ppm and Th/U ratios of 2810.08~1.11. Twelve zircon rims were dated. Among them, one analysis has a $^{206}Pb/^{238}U$ age of 28224±0.7 Ma, and the remaining eleven analyses define a discordia chord with intercept ages of 283480±34 and 1459±91 Ma (MSWD=5.8) respectively (Fig.6e). Except that two analyses have 284high Th (1666 and 1704 ppm) and Th/U (1.08 and 1.22), the rims have U of 256~3138 ppm, 285Th of 3.2~193 ppm and Th/U ratios of 0.01~0.22. It is possible that during early Paleozoic 286time, the Proterozoic sedimentary rocks underwent high-grade metamorphism which results 287in the partial loss of radiogenic Pb of inherited zircon by recrystallization. Note that the two 288~490 Ma zircon rims have high Th (1666.2 and 1703.8 ppm) and Th/U (1.08 and 1.22), 289possibly indicating a new zircon growth. Moreover, the Cenozoic age of metamorphism is 290also confirmed by a ~24 Ma U-Pb zircon age.

291

292**5. Discussion**

293**5.1 Peak-retrograde metamorphic timing**

294 The morphology (rounded and ovoid), CL images (sector, planar or homogeneous), and 295low Th/U ratios (0.01-0.1) of zircons grains or zircon domains in samples T604, T605 and

296T609 (other than the magmatic cores from T609) indicate that they are metamorphic in origin 297(Vavra et al, 1996, 1999; Hoskin and Black, 2000; Rubatto, 2002; Tomaschek et al., 2003; 298Bingen et al., 2004). The consistent ages between the zircon cores from the mafic granulite 299T605 and the zircon rims from the orthogneiss T609 lead us to assign a metamorphic event at 300ca.24 Ma. The event has also been reported by other authors (Ding and Zhong, 1999; Liu et 301al., 2007) and is common elsewhere within the Greater Himalayan Sequence of the Himalaya. 302Zircon rims from T605 and zircon grains from T604 yield two groups of younger ages of 303ca.19 Ma and ca.17 Ma, implying an upper amphibolite/lower granulite retrogression 304occurred at 19-17 Ma.

305 The ca.24 Ma zircon cores from T605 are MREE-HREE depleted, similar to values 306expected for HP metamorphic zircons that grew in competition with garnet (Fig. 8a) (Rubatto, 3072002; Whitehouse and Platt, 2003; Tomkins et al., 2005; Rubatto and Hermann 2007). The 308slightly negative or positive Eu anomalies (Eu/Eu*=0.65~1.16, cluster around 0.92) indicate 309growth in the absence of plagioclase (Rubatto, 2002). The presence of growing garnet and the 310absence of plagioclase are consistent with the HP granulite-facies assemblages (M1: 311garnet+clinopyroxene+minor quartz) in mafic granulites identified by Zhong and Ding 312(1996). Therefore, we suggest that the zircon core age of 24.0±0.3 Ma from T605 dates the 313HP granulite-facies peak metamorphism in the eastern Himalayan syntaxis. This is reinforced 314by the zircon metamorphic rim age of 24.2±0.4 Ma from the host orthogneiss (T609). A few 315cores in T605 display metamorphic ages of ca. 30 Ma, which are close to zircon metamorphic 316ages of 30~33 Ma obtained from a garnet-sillimanite gneiss in the Zhibai formation (Liu et 317al., 2007). Ding et al. (2001) proposed a HP event at ~40 Ma, which is not observed in this 318study. If ca. 24 Ma peak metamorphic age for the HP granulite-facies is correct, >30 Ma ages 319could record prograde metamorphic events. For sample T605, the ca.19 Ma zircon rims are 320chemically distinct from the cores. The rims are enriched in U (1829~2112 ppm) and Th

321(41~98 ppm) relative to the cores (U: 144~499 ppm and Th: 4~37 ppm) (Fig.7). Moreover, 322these rims have flatter MREE-HREE patterns than the cores (Fig.8) and show moderately 323negative Eu anomalies (Eu/Eu*=0.39~0.54). Accordingly, we suggest that zircon rim growth 324occurred in the presence of garnet and plagioclase (Rubatto, 2002; Whitehouse and Platt, 3252003; Tomkins et al., 2005; Rubatto and Hermann 2007), during the initial stage of garnet 326breakdown to clinopyroxene+plagioclase/amphibole+plagioclase as symplectite during the 327retrograde metamorphism of the mafic granulite (Fig.4a). Thus, 18.8±0.3 Ma could record the 328timing of the MP granulite-facies metamorphism, resulting from exhumation of the HP 329granulitic rocks.

330 The zircons from T604, an amphibolitized granulite, have high HREE concentrations and 331display steep MREE-HREE patterns, with negative Eu anomalies (Eu/Eu*=0.32-0.89). Their 332REE patterns (Fig. 8c) indicate that they formed without coexisting garnet under low-pressure 333conditions (Rubatto, 2002; Whitehouse and Platt, 2003; Tomkins et al., 2005; Rubatto and 334Hermann 2007). Accordingly, we interpret the age of 17.0±0.4 Ma to represent the timing of 335amphibolite-facies metamorphism during the exhumation of the HP mafic granulite. This age 336can be comparable with the Sm-Nd isochronal results (16.0±2.5 Ma) obtained on whole-rock 337and four garnet fractions from a metapelite (Burg et al., 1998), though it is difficult to directly 338compare these two dates as they are from different areas and dating approaches.

339 Recently, Booth et al. (2009) published U-Th-Pb monazite and titanite ages of 3-10 Ma, 340and interpret these ages to represent timing of prograde metamorphism within the Namche 341Barwa. However, these HP rocks contain complex fluid inclusion, which were trapped during 342granulite-facies metamorphism and amphibolite-facies retrogression or even later (Shen et al., 3432008). Infiltration of fluids during retrograde metamorphism is likely to cause monazite and 344titanite recrystallization (e.g., Villa, 1997; Crowley and Ghent, 1999; Townsend et al., 2000; 345Romer and Rötzler, 2003), and thus these ages probably indicate the time of retrograde fluid

infiltration (e.g., Ayers et al., 2002). Miocene and younger (13-3 Ma) anatexis occurred within the Namche Barwa syntaxis (Burg et al., 1998; Ding et al., 2001; Booth et al., 2004), which in turn may be related to decompression melting during rapid exhumation. Besides, fission-track ages of ~2.5 Ma for zircon and ~1.1 Ma for apatite recorded the following low-temperature events during exhumation within the Namche Barwa (Burg et al., 1998).

5.2 Two tectonic provinces in the eastern Himalayan syntaxis

U-Pb zircon ages and whole-rock Sm-Nd isotopic model ages (T_{DM}) of the metasedimentary rocks from the Greater Himalaya and the Lesser Himalaya reveal an important distinction between the two tectonic units (Parrish and Hodges, 1996; Whittington et al., 1999; Ahmad et al., 2000; DeCelles et al., 2000, 2004; Martin et al., 2005; Richards et al., 2005, 2006). For the Greater Himalayan Series (GHS), detrital zircon ages range from 0.8 to 2.7 Ga, with prominent peaks at 0.8-1.1, 1.5-1.7 and 2.5 Ga. By comparison, the Lesser Himalayan Series (LHS) contains detrital zircon ages ranging from ~1.6 to ~2.6 Ga with peaks at 1.8 Ga and 1.9 Ga (Parrish and Hodges, 1996; DeCelles et al., 2000, 2004; Matin et al., 2005; Richards et al., 2005, 2006). The deposition ages of the LHS and GHS could be constrained by the youngest date of detrital zircons and by the intrusion age of granite. Accordingly, the metasedimentary rocks of the LHS are most likely Early Proterozoic (~1900-1600 Ma), and the Greater Himalayan sedimentary protoliths are bracketed between Late Proterozoic and Early Ordovician (~800-480 Ma) (Parrish and Hodges, 1996; Ahmad et al., 2000; DeCelles et al., 2000, 2004; Richards et al., 2006).

As stated above, the Namche Barwa Group in the Indian plate can be subdivided into three mappable lithological subunits: Zhibai formation, Duoxiongla migmatite and Paixiang formation (Fig.1). Our previous U-Pb zircon dating work on the migmatite of the Duoxiongla unit, the core of the Namche Barwa group, shows that the melanosome has a protolith age of

3711759±10 Ma and the leucosome formed in 1594±13 Ma (Guo et al., 2008). In addition, a 372granitic gneiss from the Duoxiongla unit gave a U-Pb zircon age of 1583±6 Ma representing 373its protolith age, which is identical with the leucosome of the migmatite in age. The 1.6-1.8 374Ga tectono-magmatic events are unique in the LHS, implying that the Duoxiongla unit has an 375affinity with the LHS (Guo et al., 2008). In contrast, detrital zircons of a metasedimentary 376rock (T602) from the Zhibai formation range from ~600 to ~2000 Ma with peak at 800-1200 377Ma. The sedimentary rock could have experienced metamorphism at ~480 Ma, which is close 378to the protolith age (~490 Ma) of the orthogneiss T609. The metamorphism and partial 379melting during Paleozoic time (~490 Ma) are also identified from a garnet-kyanite gneiss by 380Liu et al. (2007). The youngest detrital zircon age from the metasedimentary rock, together 381with the orthogneiss intruded at 490 Ma, suggest that the depositional ages for the Zhibai 382formation range between 490 and ~600 Ma. According to the age distribution of the detrital 383zircons and the depositional ages, we consider that the Zhibai formation has an affinity with 384the GHS. That is to say, the HP granulite terrane should belong to the GHS. Our study shows 385that the two main tectonic provinces (the LHS and GHS) also occur in the eastern Himalayan 386syntaxis, resembling those of the western Himalayan syntaxis in Pakistan (Argles et al., 3872003).

388

389**5.3 Tectonic implication**

390 Our zircon U-Pb dating and trace element compositions from the mafic granulites and 391the host orthogneiss in the eastern Himalayan syntaxis, define the timing of HP granulite-392facies and an upper amphibolite/lower granulite-facies metamorphism at ca.24 Ma and 19-17 393Ma, respectively. In the context of the thermobarometric framework by Zhong and Ding 394(1996), the vertical exhumation rate of the Zhibai unit is between 2.5 and 10 mm/yr during the 395Early Miocene. It appears to be slower than the exhumation rate (~40 mm/yr) of the UHP

396metamorphic terrane in the western Himalayan syntaxis during the Early Eocene (Yin, 2006).

397 In the western Himalaya, coesite-bearing eclogites have been discovered in the Tso
398Morari area of NW India and upper Kaghan valley of northern Pakistan (O'Brien et al., 2001;
399Mukherjee and Sachan, 2003). Petrological and thermobarometrical evidence indicates that
400they record an ultrahigh-pressure stage at P≥27 kbar and T>690 ℃ (O'Brien et al., 2001;
401Mukherjee and Sachan, 2003). Geochronogical study shows that their peak-pressure
402metamorphism occurred in the Early Eocene (<55 Ma to ~46 Ma), and they exhumed rapidly
403to upper crust depth before ~40 Ma (de Sigoyer et al., 2000; O'Brien et al., 2001; Kaneko et
404al., 2003; Leech et al., 2005; Parrish et al., 2006; Yin, 2006). These events can be
405distinguished from underthrusting and subsequent exhumation processes of HP rocks in the
406eastern Himalaya that experienced granulite-facies metamorphism and Miocene exhumation
407(this study; Lombardo and Rolfo, 2000; Li et al., 2003; Ji et al., 2004; Groppo et al., 2007).
408These differences are probably due to different processes and the location of the UHP-HP
409rocks. The western Himalayan UHP eclogites formed in low-temperature metamorphism,
410consistent with burial along a cold geothermal gradient (de Sigoyer et al., 2000). This can be
411ascribed to the early subduction of the distal part of the Indian margin with a very rapid
412burial/exhumation cycle (de Sigoyer et al., 2000; Parrish et al., 2006). Their exhumation
413occurred along the Main Mantle Thrust (MMT)/ITSZ. However, the HP rocks in the eastern
414Himalaya are exhumated within the MCT zone or the GHS unit, farther south of the ITSZ
415(this study; Guillot et al., 2008). The ~24 Ma peak time of the HP granulites in the eastern
416Himalayan syntaxis, coupled with the prograde metamorphism at ~30 Ma or even at ~ 45 Ma
417(Catlos et al., 2002) implies slower burial than for the UHP metamorphic rocks of the NW
418Himalaya (Kaneko et al., 2003; Leech et al., 2005). They are likely related to a second phase
419of crustal thickening coherent with the India-Asian continental collision. As this HP
420metamorphism is different from the previous UHP metamorphism, it is thus reasonable that its

421peak-retrograde ages are younger. We cannot rule out the possibility that an early UHP 422metamorphic episode occurred along the ITSZ, north of the HP rocks in the eastern Himalaya. 423The record may be erased by the later thermal events related to MCT (Lombardo and Rolfo, 4242000; Groppo et al., 2007).

425 By ~24 Ma, doming occurs in the western Himalayan syntaxis and its adjacent area, 426involving the Indian crust and the Karakorum (Asian) margin (Rolland et al., 2001, 2006a, 4272006b). In the core of domes, some granulites are found which have ages in the range of ~20-42815 Ma from $^{40}Ar/^{39}Ar$ amphibole dating by Rolland et al. (2006b). The phase of 429metamorphism may have initiated as early as 25 Ma in the Baltoro area (Rolland et al., 2001). 430Thus, the peak-retrograde metamorphism of 24-17 Ma in the eastern Himalayan syntaxis is 431coherent with evolution of the western Himalayan syntaxis. Note that the age of ~24 Ma is 432also the timing of the initiation of exhumation of the GHS (e.g., Hodges, 2000; Yin, 2006), in 433agreement with initiation of the MCT (e.g., Daniel et al., 2003; Harris et al., 2004). Then the 434whole metamorphic history of the Himalayan belt becomes similar at ~24 Ma. The phase of 435metamorphism is spatially and temporarily associated with magmatism involving some 436asthenospheric component in the western Himalayan syntaxis (Rolland et al., 2001). This is in 437good agreement with ~24 Ma granites emplacement after a magmatic quiescent period of ~15 438Ma along the suture zone west and north of Namche Barwa (Fig.1) (Booth et al., 2004). 439Therefore, a common process can be invoked for the metamorphic and magmatic evolution. 440The most likely cause is a slab breakoff occurring at ~24 Ma (Rolland et al., 2001; Mahéo et 441al. 2002) (Fig. 9). The slab breakoff could also explain the onset of exhumation at ~24 Ma, as 442suggested by Rolland et al. (2001).

443

444**Conclusions**

445 A combination of zircon U-Pb ages and trace element, and petrology for the mafic

446granulites and their host orthogneiss in the eastern Himalayan syntaxis provide chronological 447constraints on the HP granulite-facies and upper amphibolite/lower granulite-facies 448metamorphism. The peak metamorphic age for the HP granulite is at ~24 Ma and subsequent 449moderate- and low-pressure retrograde metamorphism occurred at 19-17 Ma. The HP 450metamorphic events are significantly different from the UHP metamorphic events in the 451western Himalaya, but their metamorphic history becomes relatively similar after ~24 Ma. 452The distribution of detrital zircon ages and the depositional age of the Zhibai formation 453provide a strong evidence that the granulite terrane has affinity with the GHS.

454

455**Acknowledgements**

456This research was supported by the Natural Science Foundation of China (grants: 40821061 457and 40773019) and by the Ministry of Education of China and the State Administration of 458Foreign Expert Affairs of China (Grant B07039) and by Opening Foundation of the State Key 459Laboratory of Geological Process and Mineral Resourse. We thank Prof. Y. Rolland, an 460anonymous reviewer for their constructive comments that greatly improved this manuscript. 461We also thank Dr. Yuan-Bao Wu for his helpful discussion.

462

463**References**

464

465Ahmad, T., Harris, N., Bickle, M., Chapman, H., Bunbury, J., Prince, C., 2000. Isotopic 466 constrains on the structural relationships between the Lesser Himalayan Series and High 467 Himalayan Crystalline Series, Garhwal Himalaya. GSA Bulletin 112, 467-477.

468Andersen T., 2002. Correction of common lead in U-Pb analyses that do not report ^{204}Pb. 469 Chemical Geology 192, 59-79.

470Argand, E., 1924. La tectonique de l'Asie. International Geological Congress, 13th.

471 Proceedings 7, 171-372.

472Argles, T., Foster, G., Whittington, A., Harris, N., George, M., 2003. Isotope studies reveal a
473 complete Himalayan section in the Nanga Parbat syntaxis. Geology 31, 1109-1112.

474Ayers, J.C., Dunkle, S., Gao, S., Miller, C.F., 2002. Constraints on timing of peak and
475 retrograde metamorphism in the Dabie Shan Ultrahigh-Pressure Metamorphic Belt, east-
476 central China, using U-Th-Pb dating of zircon and monazite. Chemical Geology 186, 315-
477 331.

478Berman, R.G., 1990. Mixing properties of Ca-Mg-Fe-Mn garnet. American Mineralogist 75,
479 328-344.

480Bingen, B., Austrheim, H., Whitehouse, M.J., Davis, W.J., 2004. Trace element signature and
481 U-Pb geochronology of eclogite-facies zircon, Bergen Arcs, Caledonides of W Norway.
482 Contributions to Mineralogy and Petrology 147, 67-683.

483Booth, A.L., Zeitler, P.K., Kidd, W.S.F., Wooden, J., Liu, Y.P., Idleman, B., Hern, M.,
484 Chamberlain, C.P., 2004. U-Pb zircon constrains on the tectonic evolution of southeastern
485 Tibet, Nacmche Barwa area. American Journal of Science 304, 889-929.

486Booth, A.L., Chamberlain, C.P., Kidd, W.S.F., Zeitler, P.K., 2009. Constraints on the
487 metamorphic evolution of the eastern Himalayan syntaxis from geochronologic and
488 petrologic studies of Namche Barwa. GSA Bulletin 121, 385-407.

489Burg, J.P., Davy, P., Nievergelt, P., Oberli, F., Seward, D., Diao, Z.Z., Meier, M., 1997.
490 Exhumation during crustal folding in the Namche-Barwa syntaxis. Terra Nova 9, 53-56.

491Burg, J.P., Nievergelt, P., Oberli, F., Seward, D., Davy, P., Maurin, J.C., Daio, Z.Z., Meier, M.,
492 1998. The Namche Barwa syntaxis: evidence for exhumation related to compressional
493 crustal folding. Journal of Asian Earth Sciences 16, 239-252.

494Catlos, E.J., Harrison, T.M., Manning, C.E., Grove, M., Rai, S.M., Hubbard, M., Upreti, B.N.,
495 2002. Records of the evolution of the Himalayan orogen rom in situ Th-Pb ion microprobe

496 dating of the monazite: eastern Nepal and western Garhwal. Journal of Asian Earth
497 Sciences 20, 459-479.

498Corfu, F., Hanchar, J.M., Hoskin, P.W.O., Kinny, P., 2003. Altas of zircon textures. Reviews in
499 Mineralogy and Geochemistry 53, 469-500.

500Chiu, H.Y., Chung, S.L., Wu, F.Y., Liu, D.Y., Liang, Y.H., Lin, I.J., Iizuka, Y., Xie, L.W.,
501 Wang, Y.B., Chu, M.F., 2009. Zircon U-Pb and Hf isotopic constraints from eastern
502 Transhimalayan batholiths on the precollisional magmatic and tectonic evolution in
503 southern Tibet. Tectonophysics 477, 3-19.

504Chung, S.L., Liu, D.Y., Ji, J.Q., Chu, M.F., Lee, H.Y., Wen, D.J., Lo, C.H., Lee, T.Y., Qian,
505 Q., Zhang, Q., 2003. Adakites from continental collision zones: Melting of thickened
506 lower crust beneath southern Tibet. Geology 31, 1021-1024.

507Crowley, J.L., Ghent, E.D., 1999. An electron microprobe study of the U-Th-Pb systematics
508 of metamorphosed monazite: the role of Pb diffusion versus overgrowth and
509 recrystallization. Chemical Geology 157, 285-302.

510Daniel, C.G., Hollister, L.S., Parrish, R.R., Grujic, D., 2003. Exhumation of the main central
511 thrust from lower crustal depths, eastern Bhutan Himalaya. J. metamorphic Geol. 21, 317-
512 334.

513Davis, D.W., 2002. U-Pb geochronology of Archean metasedimentary rocks in the Pontiac
514 and Abitibi subprovinces, Quebec, constraints on timing, provenance and regional
515 tectonics. Precambrian Research 115, 97-117.

516de Sigoyer, J., Chavagnac, V., Blichert-Toft, J., Villa, I.M., Luais, B., Guillot, S., Cosca, M.,
517 Mascle, G., 2000. Dating the Indian continental subduction and collisional thickening in
518 the northwest Himalaya: Multichronology of the Tso Morari eclogites. Geology 28, 487-
519 490.

520DeCelles, P.G., Gehrels, G.E., Quade, J., Lareau, B., Spurlin, M., 2000. Zircon ages of the

521 Himalayan orogenic belt in Nepal. Science 288, 497-499.

522DeCelles, Gehrels, G.E., Najman, Y., Martin, A.J., Carter, A., Garzanti, E., 2004. Detrital
523 geochronology and geochemistry of Cretaceous-Early Miocene strata of Nepal:
524 implication for timing and diachroneity of initial Himalayan orogenesis. Earth and
525 Plaentary Science Letters 227, 313-330.

526Ding, L., Zhong, D.L., 1999. Metamorphic characteristics and geotectonic implications of the
527 high-pressure granulites from Namjagbarwa, eastern Tibet. Science in China (Series D)
528 42, 491-505.

529Ding, L., Zhong, D.L., Yin, A., Kapp, P., Harrison, T.M., 2001. Cenozoic structureal and
530 metamorphic evolution of the eastern Himalayan syntaxis (Namche Barwa). Earth and
531 Planetary Science Letters 192, 423-438.

532Ellis, D.J., Green, D.H., 1979. An experimental study of the effect of Ca upon garnet-
533 clinopyroxene Fe-Mg exchange equilibria. Contributions to Mineralogy and Petrology 71,
534 13-22.

535Gansser, A., 1964. The geology of the Himalayas. Wiley Interscience, New York, 289.

536Geng, Q.R., Pan, G.T., Zheng, L.L., Sun, Z.M., Qu, C.S., Dong, H., 2004. Petrological
537 characteristics and original settings of the Yarlung Tsangpo ophiolitic mélange, Namche
538 Barwa, SE Tibet. Chinese Journal of Geology 39, 1-19 (in Chinese with English abstract).

539Geng, Q.R., Pan, G.T., Zheng, L.L., Chen, Z.L., Fisher, R.D., Sun, Z.M., Ou, C.S., Dong, H.,
540 Wang, X.W., Li, S., Lou, X.Y., Fu, H., 2006. The eastern Himalayan syntaxis: major
541 tectonic domains, ophiolitic mélanges and geologic evolution. Journal of Asian Earth
542 Sciences 27, 265-285.

543Groppo, G., Lombardo, B., Rolfo, F., Pertusati, P., 2007. Clockwise exhumation path of
544 granulitized eclogites from the Ama Drime range (Eastern Himalayas). Journal of
545 Metamorphic Geology 25, 51-75.

546Guillot, S., de Sigoyer, J., Lardeaux, J.M., Mascle, G., 1997. Eclogitic matasediments from
547 the Tso Morari (Ladakh, Himalaya): evidence for continental subduction during India-
548 Asia convergence. Contributions to Mineralogy and Petrology 128, 197-212.
549Guillot, S., Mahéo, G., de Sigoyer, J., Hattori, K.H., Pecher, A., 2008. Tethyan and Indian
550 subdution viewed from the Himalayan high- to ultrahigh-pressure metamorphic rocks.
551 Tectonophysics 451, 225-241.
552Guo, L., Zhang, H.F., Xu, W.C., 2008. U-Pb zircon ages of migmatite and granitic gneiss from
553 Duoxiongla in eastern Himalayan syntaxis and their geological implications. Acta
554 Petrologica Sinica 24, 421-429 (in Chinese with English abstract).
555Harris, N.B.W., Caddick, M., Kosler, J., Goswami, S., Vance, D., Tinale, A.G., 2004. The
556 pressure-temperature-time path of migmatites from the Sikkim Himalaya. J. metamorphic
557 Geol. 22, 249-264.
558Harley, S., 1984. An experimental study of the partitioning of Fe and Mg between garnet and
559 orthopyroxene. Contributions to Mineralogy and Petrology 86, 359-373.
560Hermann, J., Rubatto, D., Korsakov, A., 2001. Multiple zircon growth during fast exhumation
561 of diamondiferous, deeply subducted continental crust (Kokchetav Massif, Kazakhstan).
562 Contributions to Mineralogy and Petrology 141, 66-82.
563Hodges, K.V., Spear, F.S., 1982. Geothermometry, geobarometry and the Al_2SiO_5 triple point
564 at Mt. Moosilauke, New Hampshire. American Mineralogist 67, 1118-1134.
565Hodges, K.V., 2000. Tectonics of the Himalaya and southern Tibet from two perpectives. GSA
566 Bulletin 112, 324-350.
567Hoskin, P.W.O., Black, L.P., 2000. Metamorphic zircon formation by solid-state
568 recrystallization of protolith igneous zircon. Journal of Metamorphic Geology 18, 423-
569 439.
570Ji, J.Q., Zhong, D.L., Song, B., Chu, M.F., Wen, D.J., 2004. Metamorphism, geochemistry

571 and U-Pb zircon SHRIMP geochronology of the high-pressure granulites in the central
572 Greater Himalayas. Acta Petrologica Sinica 20, 1283-1300 (in Chinese with English
573 abstract).

574Kaneko, Y., Katayama, I., Yamamoto, H., Misawa, K., Ishikawa, M., Rehman, H.U., Kausar,
575 A.B., Shiraishi, K., 2003. Timing of Himalayan ultrahigh-pressure metamorphism: sinking
576 rate and subduction angle of the Indian continental crust beneath Asia. Journal of
577 Metamorphic Geology 21, 589-599.

578Kroll, H., Evangelakakis, C., Voll, G., 1993. Two-feldspar geothermometry: a review and
579 revision for slowly cooled rocks. Contributions to Mineralogy and petrology 114, 510-
580 518.

581Leech, M.L., Singh, S., Jain, A.K., Klemperer, S. L., Manickavasagam, R.M., 2005. The onset
582 of India-Asia continental collision: Early, steep subduction required by the timing of UHP
583 metamorphism in the western Himalaya. Earth and Planetary Science Letters 234, 83-97.

584Li, D.W., Liao, Q.A., Yuan, Y.M., Wang, Y.S., Liu, D.M., Zhang, X.H., Yi, X.H., Cao, S.Z.,
585 Xie, D.F., 2003. SHRIMP U-Pb zircon geochronology granulites at Rimana (southern
586 Tibet) in the central segment of Himalayan Orogen. Chinese Science Bulletin 48, 2647-
587 2650.

588Liu, Y., Zhong, D.L., 1997. Petrology of high-pressure granulites from the eastern Himalayan
589 syntaxis. Journal of Metamorphic Geology 15, 451-466.

590Liu, Y., Yang, Z.Q., Wang, M., 2007. History of zircon growth in a high-pressure granulite
591 within the eastern Himalayan syntaxis and tectonic implications. International Geology
592 Review 49, 861-872.

593Lombardo, B., Rolfo, F., 2000. Two contrasting eclogite types in the Himalayas: implications
594 for the Himalayan orogeny. Journal of Geodynamics 30, 37-60.

595Ludwig, K.R., 2003. User's manual for Isoplot 3.0: A geochronological toolkit for Microsoft

596 Excel Berkeley geochronology center. Special publication 4, 1-77.

597Mahéo, G., Guillot, S., Blichert-Toft, J., Rolland, Y., Pêcher, A., 2002. A slab breakoff model
598 for the Neogene thermal evolution of south Karakorum and South Tibet. Earth and
599 Planetary Science Letters 195, 45-58.

600Martin, A.J., DeCelles, P.G., Gehrels, G.E., Patchett, P.J., Isachsen, C., 2005. Isotopic and
601 structural constraints on the location of the Main Central thrust in the Annapurna Range,
602 central Nepal Himalaya. GSA Bulletin 117, 926-944.

603Mukherjee, B.K., Sachan, H.K., Ogasawara, Y., Muko, A., Yoshioka, N., 2003. Carbonate-
604 bearing UHPM rocks from the Tso-Morari region, Ladakh, India: petrological
605 implications. International Geology Review 45, 49-69.

606Newton, R.C., Haselton, H.T., 1981. Thermodynamics of the garnet-plagioclase-Al_2SiO_5-
607 quartz geobarometer. In: Newton R C, Navrotsky, A. Wood, B J, eds. Thermodynamics of
608 Minerals and Melts. New York: Springer-Verlag, 131-147.

609O'Brien, P.J., Zotov, N., Law, R., Khan, M.A., Jan, M.Q., 2001. Coesite in Himalayan
610 eclogite and implications for models of India-Asia collision. Geology 29, 435-438.

611Parrish, R.R., Hodges, K.V., 1996. Isotopic constraints on the age and provenance of the
612 Lesser and Greater Himalayan sequences, Nepalese Himalaya. GSA Bulletin 108, 904-
613 911.

614Parrish, R.R., Gough, S.J., Searle, M.P., Waters, D.J., 2006. Plate velocity exhumation of
615 ultrahigh-pressure eclogites in the Pakistan Himalaya. Geology 34, 989-992.

616Perchuk, L., 1966. Relationship of temperature and Ca-distribution in coexisting of
617 amphibolite and plagioclase. Reports of Science Academy of USSR 60, 1436-1438.

618Plyusnina, L., 1982. Geothermometry and geobarometry of plagioclase-hornblende bearing
619 assemblages. Contributions to Mineralogy and Petrology 80, 140-146.

620Richards, A., Argles, T., Harris, N., Parrish, R., Ahmad, T., Darbyshire, F., Draganites, E.,

621 2005. Himalayan architecture constrained by isotopic tracers from clastic sediments. Earth
622 and Planetary Science Letters 236, 773-796.
623Richards, A., Parrish, R., Harris, N., Argles, T., Zhang, L., 2006. Correlation of lithotectonic
624 units across the eastern Himalaya, Bhutan. Geology 34, 341-344.
625Rolland, Y., Mahéo, G., Guillot, S., Pecher, A., 2001. Tectono-metamorphic evolution of the
626 Karakorum metamorphic complex (Dassu-Askole area, NE Pakistan): exhumation of mid-
627 crustal HT-MP gneisses in a convergent context. J. metamorphic Geol. 19, 717-737.
628Rolland, Y., Carrio-Schaffhauser, E., Sheppard, S.M.F., Pêcher, A., Esclauze, L., 2006a.
629 Metamorphic zoning and geodynamic evolution of an inverted crustal section (Karakorum margin, N
630 Pakistan), evidence for two metamorphic events. Int. J. Earth Sci. 95, 288-305.
631Rolland, Y., Villa, I.M., Guillot, S., Mahéo, G., Pêcher, A., 2006b. Evidence for pre-Cretaceous history
632 and partial Neogene (19-9 Ma) reequilibration in the Karakorum (NW Himalayan Syntaxis) from ^{40}Ar-
633 ^{39}Ar amphibole dating. Journal of Asian Earth Sciences 27, 371-391.
634Romer, R.L., Rötzler, J., 2003. Effect of metamorphic reaction history on the U-Pb dating of
635 titanite. Geological Society, London, Special Publications 220, 147-158.
636Rubatto, D., 2002. Zircon trace element geochemistry: partitioning with garnet and the link
637 between U-Pb ages and metamorphism. Chemical Geology 184, 123-138.
638Rubatto, D., Hermann, J., 2007. Zircon behaviour in deeply subducted rocks. Elements 3, 31-
639 35.
640Shen, K., Zhang, Z.M., Yan, L., Wang, J.L., 2008. Composition and evolution of fluids in the
641 continental orogen: A study of fluid inclusions in high-pressure granulites from the
642 Namche Barwa area, Tibet of southwest China. Acta Petrologica Sinica 24, 1488-1500 (in
643 Chinese with English abstract).
644Sun, S.S., McDonoud, W.F., 1989. Chemical and isotopic systematics of oceanic basalts:
645 implications for mantle composition and processes. In: Saunders, S.D., Norry, M.J.(Eds.),
646 Magmatism in the Ocean Basins. Geological Society, London, Special Publications 42,

647 313-345.

648Tomaschek, F., Kennedy, A.K., Villa, I.M., Markus, L., Chris, B., 2003. Zircons from Syros,
649 Cyclades, Greece-recrystallizaion and mobilization of zircon during high-pressure
650 metamorphism. Journal of Petrology 44, 1977-2002.

651Tomkins, H.S., Williams, I.S., Ellis, D.J., 2005. In situ U-Pb dating of zircon formed from
652 retrograde garnet breakdown during decompression in Rogaland, SW Norway. Journal of
653 Metamorphic Geology 23, 201-215.

654Tonarini, S., Villa, I., Oberli, F., Meier, M., Spencer, D.A., Pognante, U., Ramsay, J.G., 1993.
655 Eocene age of eclogite metamorphism in the Pakistan Himalaya implications for India-
656 Euransian collision. Terra Nova 5, 13-20.

657Townsend, K.J., Miller, C.F., D'Andrea, J.L., Ayers, J.C., Harrison, T.M., Coath, C.D., 2000.
658 Low temperature replacement of monazite in the Ireteba granite, Southern Nevada:
659 geochronological implications. Chemical geology 172, 95-112.

660Vavra, G., Gebauer, D., Schmid, R., 1996. Multiple zircon growth and recrystallization during
661 polyphase Late Carboniferous to Triassic metamorphism in granulites of the Ivrea Zone
662 (Southern Alps): an ion microprobe (SHRIMP) study. Contributions to Mineralogy and
663 Petrology 122, 337-358.

664Vavra, G., Schmid, R., Gebauer, D., 1999. Internal morphology, habit and U-Th-Pb
665 microanalysis of amphibolite-to-granulite facies zircons: geochronology of the Ivrea Zone
666 (Southern Alps). Contributions to Mineralogy and Petrology 134, 380-404.

667Wells, P.R.A., 1979. P-T condition in the Moines of the central Highlands, Scotland. Journal
668 of the Geological Society of London 136, 663-671.

669Whitehouse, M.J., Platt, J.P., 2003. Dating high-grade metamorphism-constrains from rare-
670 earth elements in zircon and garnet. Contributions to Mineralogy and Petrology 145, 61-
671 74.

672Whittington, A., Foster, G., Harris, N., Vance, D., Ayres, M., 1999. Lithostratigraphic
673 correlations in the western Himalaya: An isotopic approach. Geology 27, 585-588.
674Villa, I.M., 1997. Isotopic closure. Terra Nova 10, 42-47.
675Wood, B., Banno, S., 1973. Garnet-orthopyroxene and orthopyroxene-clinopyroxene
676 relationships in simple and complex systems. Contributions to Mineralogy and Petrology
677 42, 109-124.
678YIGS (Yunnan Institute of Geological Survey), 2005. Progress on the geological investigation
679 of 1:250,000 Nyingchi Sheet in Xizang. Sedimentary Geology and Tethyan Geology 25,
680 111-114 (in Chinese with English abstract).
681Yin, A., 2006. Cenozoic tectonic evolution of the Himalayan orogen as constrained by along-
682 strike variation of structural geometry, exhumation history, and foreland sedimentation.
683 Earth Science Reviews 76, 1-131.
684Yuan, H.L., Gao, S., Liu, X.M., Li, H.M., Gunther, D., Wu, F.Y., 2004. Accurate U-Pb age and
685 trace element determinations of zircon by laser ablation-inductively coupled plasma-mass
686 spectrometry. Geostandards and Geoanalytical Research 28, 353-370.
687Zeitler, P.K., Meltzer, A.S., Koons, P.O., Craw, D., Hallet, B., Chamberlain, C.P., Kidd,
688 W.S.F., Park, S.K., Seeber, L., Bishop, M., Shroder, J., 2001. Erosion, Himalayan
689 geodynamics, and the geomorphology of metamorphism. GSA Today 11, 4-9.
690Zhai, M.G., Guo, J.H., Yan, Y.H., 1992. The discovery and primary study of the high-pressure
691 from North China. Science in China (Series B) 35, 1325-1330 (in Chinese).
692Zhang, J.J., Ji, J.Q., Zhong, D.L., Ding, L., He, S.D., 2004. Structural pattern of eastern
693 Himalayan syntaxis in Namjagbarwa and its formation process. Science in China (D) 47,
694 138-150.
695Zhang, Z.M., Zheng, L.L., Wang, J.L., Zhao, X.D., Shi, C., 2007. Garnet pyroxenite in the
696 Namjagbarwa Group-complex in the eastern Himalayan tectonic syntaxis, Tibet, China:

697 Evidence for subduction of the Indian continent beneath the Eurasian plate at 80-100 km
698 depth. Geological Bulletin of China 26, 1-12 (in Chinese with English abstract).
699Zhang, H.F., Xu, W.C., Zong, K.Q., Yuan, H.L., Harris, N., 2008. Tectonic evolution of
700 metasediments from the Gangdise terrane, Asian plate, eastern Himalayan syntaxis, Tibet.
701 International Geology Review 50, 914-930.
702Zhong, D.L., Ding, L., 1996. Discovery of high-pressure basic granulite in Namjabarwa area,
703 Tibet, China. Chinese Science Bulletin 41, 87-88.

704
705Figure Captions

706

707Fig.1 Sketch map of (a) the Himalaya orogen and (b) the eastern Himalayan syntaxis,
708showing sample location (modified after Burg et al. (1998) and Geng et al. (2006)). Zircon U-
709Pb ages are from Ding et al. (2001), Chung et al. (2003), Booth et al. (2004), Zhang et al.
710(2008) and Chiu et al. (2009). JSS=Jinsha suture zone; BNS=Bangong-Nujiang suture zone;
711IYS=Indus-Yarlung suture zone; STDS=South Tibetan detachment system; MCT=Main
712Central thrust; KF=Karakorum fault; QT=Qiangtang terrane; LB=Lhasa terrane; TH=Tethyan
713Himalaya belt; GH=the Greater Himalaya belt; LH=the Lesser Himalaya belt; WHS=the
714western Himalayan syntaxis; EHS=the eastern Himalayan syntaxis.

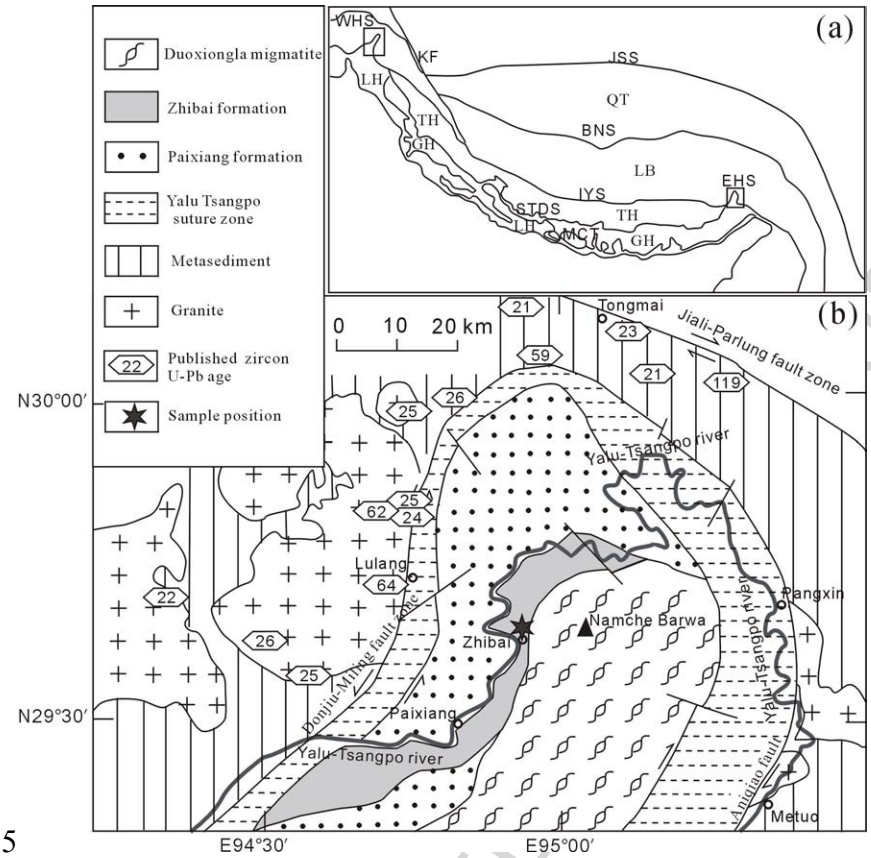

715

716Fig.2 Field view of gneiss containing mafic granulite boudins in the valley of Bulong, ~1 km

717north of Zhibai.

718

719Fig.3 P-T-t paths of the HP Namche Barwa complex and UHP Tso Morari and Kaghan units

720(modified after Guillot et al., 2008). See text for references. Abbreviations: Cpx-

721clinopyroxene, Opx-orthopyroxene, Grt-garnet, Ky-kyanite, Lws-lawsonite.

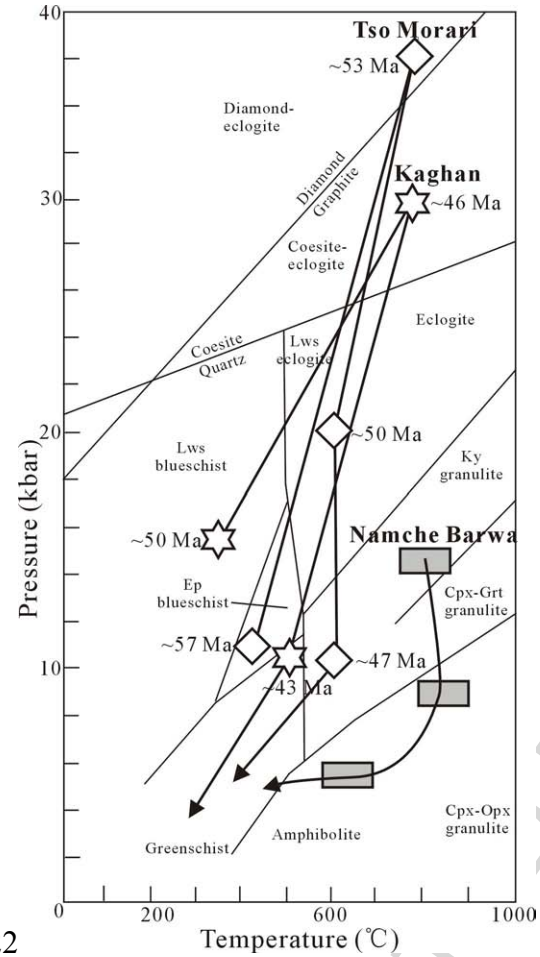

722

723Fig.4 Microstructures of (a) the weakly retrograde granulite T605, the inset show that the
724large garnet surrounded by a plagioclase-clinopyroxene and plagioclase-amphibole, set in the
725symplectite of plagioclase+orthopyroxene+clinopyoxene after garnet; (b) the amphibolitised
726granulite T604; (c) the orthogneiss T609 and (d) the high-grade metasedimentary rock T602.
727Grt=garnet, Amp=amphibole, Pl=plagioclase, Ilm=ilmenite, Bi=biotite, Qz=quartz, Kfs=K-
728feldspar.

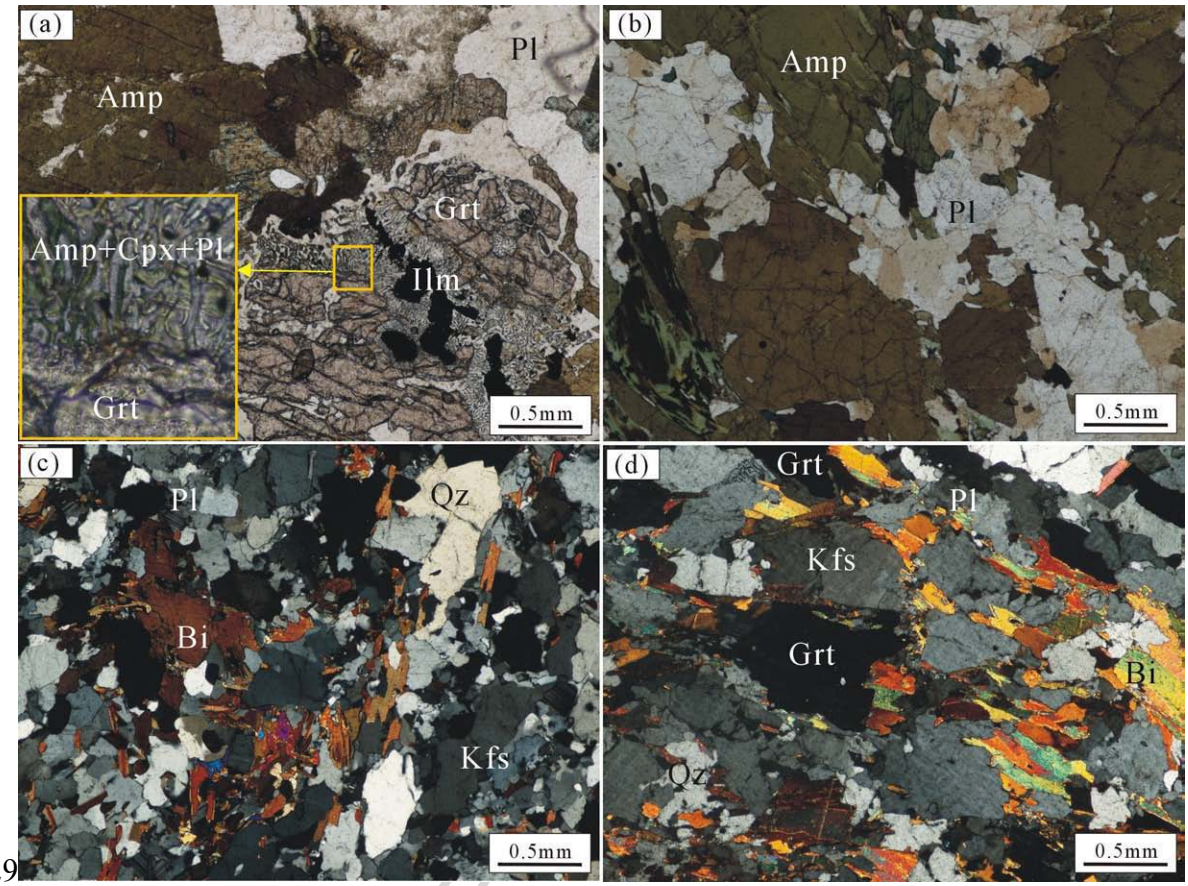

729

730Fig.5 Representative cathodoluminescence images of zircons from (a) the weakly retrograde
731mafic granulite sample T605, (b) the amphibolitised granulite sample T604, (c) the
732orthogneiss sample T609, and (d) the high-grade metasedimentary rock T602. The circles
733show LA-ICP-MS dating spots and corresponding apparent ages.

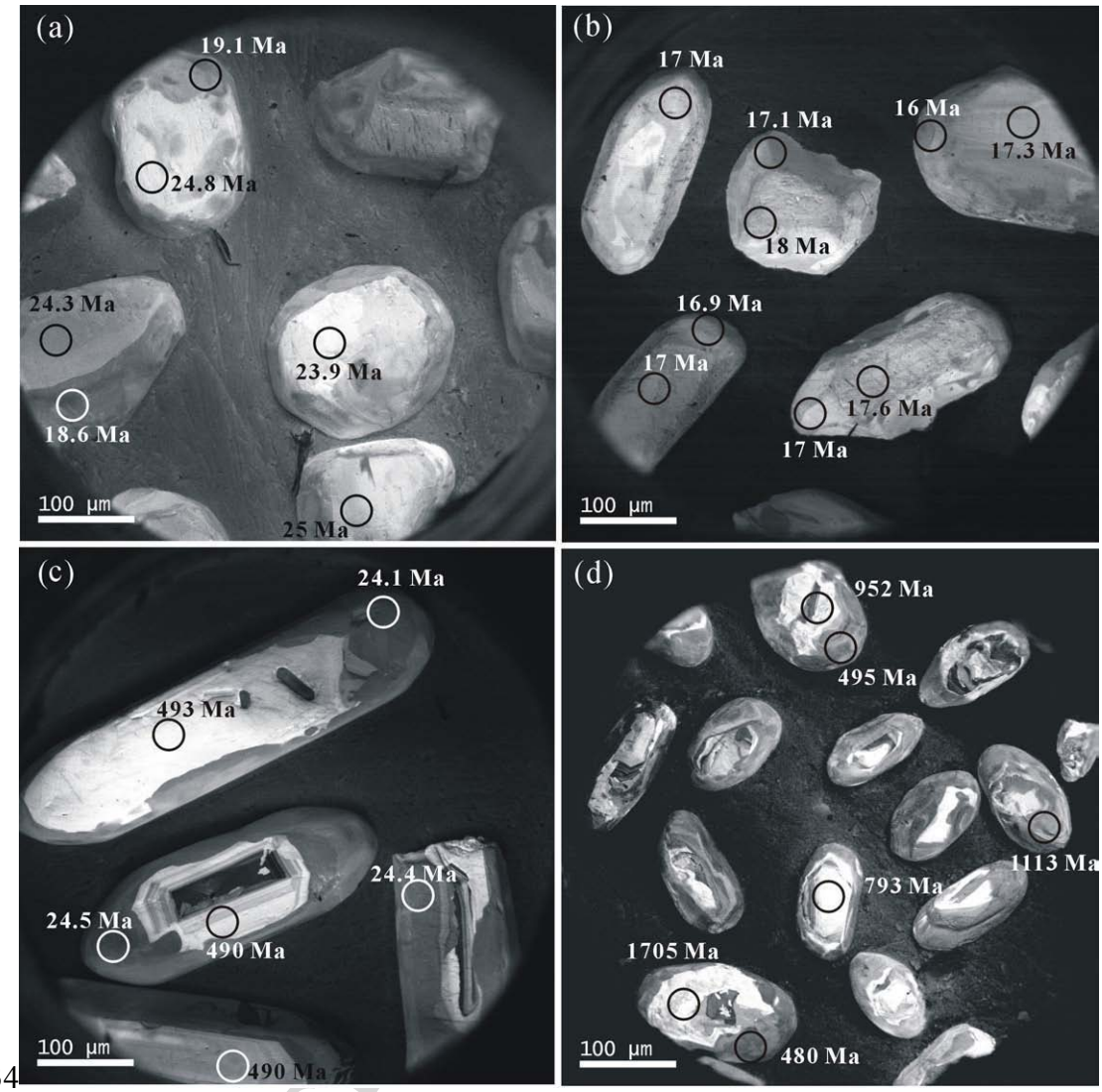

734

735Fig.6 Concordia diagrams of LA-ICP-MS U-Pb dating for zircons from (a) T605, (b) T604,

736(c, d) T609 and (e) T602. (f) U-Pb age distribution histogram for sample T602, the $^{207}Pb/^{206}Pb$

737ages for those >800 Ma and the $^{206}Pb/^{238}U$ ages for those <800 Ma.

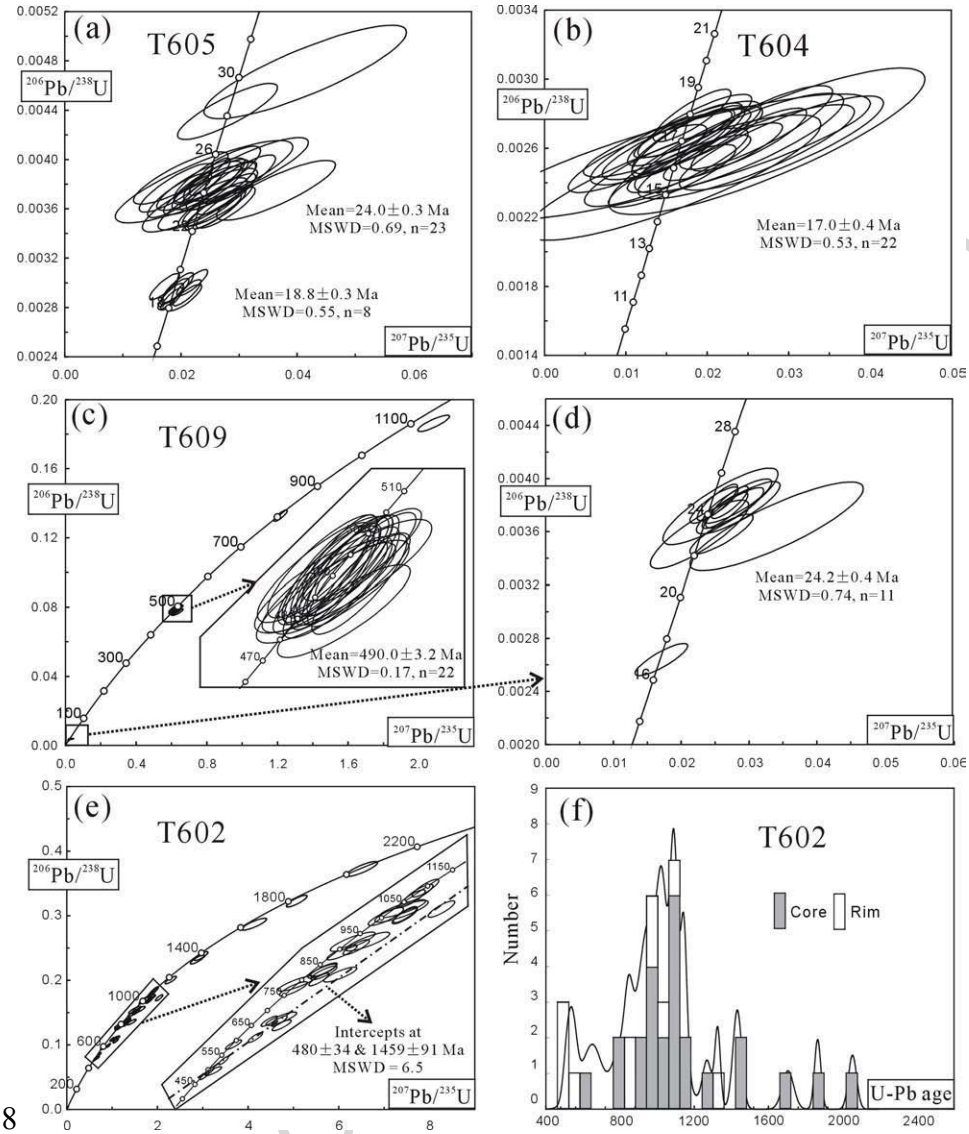

738

739Fig.7 Th versus U plot for the two granulites (T604 and T605) in the eastern Himalayan

740syntaxis.

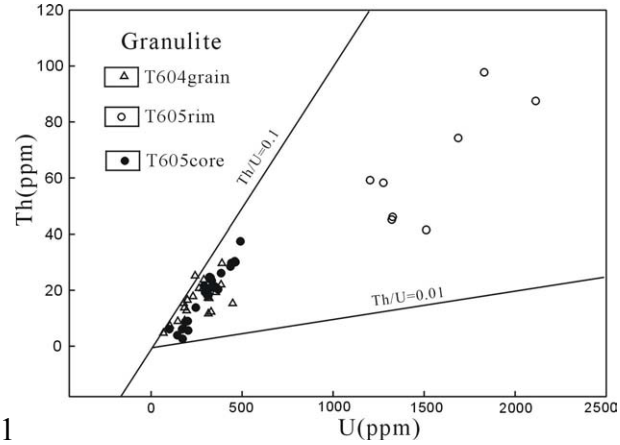

741

742Fig.8 Chondrite-normalised REE patterns for zircons from the mafic granulites in the eastern

743Himalayan syntaxis. (a) the ~24 Ma zircon cores from sample T605, (b) the ~19 Ma zircon
744rims from sample T605, (c) the ~17 Ma zircon grains from sample T604. Normalising values
745are from Sun and McDonoud (1989). The magmatic, LP and HP plots for comparison are
746from Rubatto and Hermann (2007). LP=low-pressure, HP=high-pressure

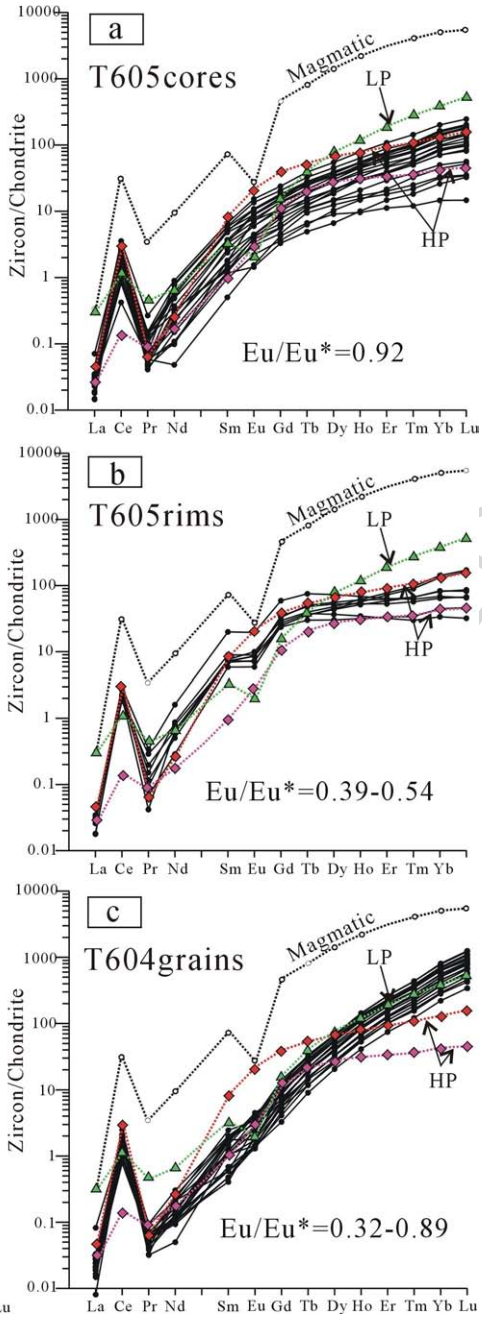

747

748Fig.9 Proposed geodynamic model of the eastern Himalayan syntaxis inferred from the
749analytical results obtained in this study. The India-Asian continental collision time for
750maximum burial of the eastern Himalayan syntaxis continental crust is at ~24 Ma, followed

751by extrusion and/or exhumation that result from a slab breakoff of the Indian plate.

752MCT=Main Central Thrust.

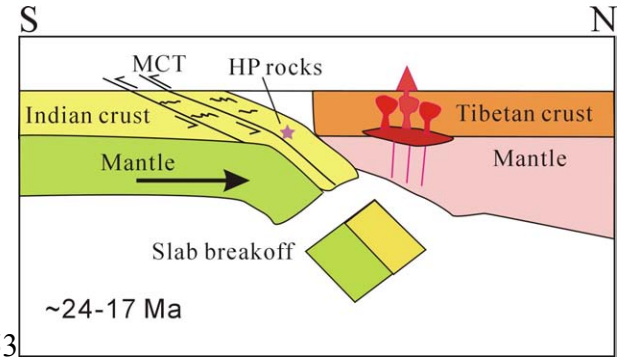

753

754

755

Table 1. Zircon U-Pb isotopic data obtained by LA-ICP-MS in the eastern Himalayan syntaxis.

Analysis	Th	U	Th/U	Isotopic ratios						Apparent ages (Ma)					
				$^{207}Pb/^{206}Pb$	1σ	$^{207}Pb/^{235}U$	1σ	$^{206}Pb/^{238}U$	1σ	$^{207}Pb/^{206}Pb$	1σ	$^{207}Pb/^{235}U$	1σ	$^{206}Pb/^{238}U$	1σ
T605 weakly retrograde granulite															
1r	41.5	1511.4	0.03	0.05311	0.00436	0.02193	0.00176	0.003	0.00007	333	140	22	2	19.3	0.4
2c	26.1	383.9	0.07	0.05012	0.00731	0.02499	0.00358	0.00362	0.00011	201	259	25	4	23.3	0.7
3c	6.1	99.3	0.06	0.06375	0.01802	0.04139	0.01151	0.00471	0.00025	733	488	41	11	30	2
4r	58.3	1275.3	0.05	0.05228	0.00413	0.02105	0.00159	0.00292	0.00007	298	182	21	2	18.8	0.4
5c	24.7	320.4	0.08	0.05162	0.0078	0.02696	0.004	0.00379	0.00013	269	267	27	4	24.4	0.8
6c	37.5	490.2	0.08	0.05568	0.00689	0.0277	0.00336	0.00361	0.00011	440	216	28	3	23.2	0.7
7c	18.3	314.8	0.06	0.04772	0.00813	0.02516	0.00424	0.00382	0.00012	85	273	25	4	24.6	0.8
8c	20.9	330.3	0.06	0.05668	0.00801	0.02999	0.00415	0.00384	0.00013	479	248	30	4	24.7	0.8
9c	30.1	462.9	0.06	0.04689	0.00444	0.02495	0.00232	0.00386	0.0001	44	156	25	2	24.8	0.6
10c	8.8	188.7	0.05	0.04736	0.01023	0.02375	0.00507	0.00364	0.00014	67	319	24	5	23.4	0.9
11c	2.6	172.8	0.02	0.04621	0.00947	0.028	0.00567	0.00439	0.00015	9	303	28	6	28.2	1
12c	6.1	170.3	0.04	0.03758	0.01018	0.01997	0.00537	0.00385	0.00014	-435	373	20	5	24.8	0.9
13c	5.6	203.3	0.03	0.04904	0.00933	0.02624	0.00492	0.00388	0.00015	150	302	26	5	25	1
14c	30.4	458.8	0.07	0.03864	0.00717	0.01976	0.00363	0.00371	0.00012	-370	263	20	4	23.9	0.8
15c	13.8	244.9	0.06	0.03695	0.00816	0.01918	0.0042	0.00377	0.00013	-475	337	19	4	24.3	0.8
16r	59.2	1202.5	0.05	0.04569	0.0037	0.01823	0.00145	0.00289	0.00007	-18	128	18	1	18.6	0.4
17c	18.3	307.8	0.06	0.05244	0.00814	0.0263	0.00402	0.00364	0.00012	305	280	26	4	23.4	0.8
18c	9.0	201.0	0.04	0.04468	0.0097	0.02342	0.00503	0.0038	0.00014	-36	294	24	5	24.4	0.9
19r	97.8	1829.2	0.05	0.0466	0.00331	0.01843	0.00129	0.00287	0.00006	29	113	19	1	18.5	0.4
20c	29.8	440.3	0.07	0.05172	0.00658	0.02556	0.0032	0.00358	0.0001	273	230	26	3	23	0.6
21c	20.3	367.7	0.06	0.05271	0.00679	0.02616	0.0033	0.0036	0.00011	316	228	26	3	23.2	0.7
22c	3.9	144.0	0.03	0.07038	0.01337	0.03636	0.00676	0.00375	0.00016	939	325	36	7	24	1
23c	28.5	435.7	0.07	0.05428	0.0066	0.02784	0.00332	0.00372	0.00011	383	214	28	3	23.9	0.7
24r	46.1	1326.7	0.03	0.04683	0.0041	0.0189	0.00163	0.00293	0.00007	41	145	19	2	18.9	0.4
25c	24.5	326.7	0.07	0.05053	0.00841	0.02635	0.00431	0.00378	0.00013	219	285	26	4	24.3	0.8
26c	21.3	349.9	0.06	0.04673	0.00767	0.02443	0.00395	0.00379	0.00013	35	252	25	4	24.4	0.8
27r	87.5	2112.3	0.04	0.05223	0.0048	0.02074	0.00187	0.00288	0.00007	295	160	21	2	18.5	0.4

756

28c	21.6	290.8	0.07	0.05768	0.01333	0.03118	0.0071	0.00392	0.00017	518	399	31	7	25	1
29c	19.3	296.1	0.07	0.04605	0.01312	0.02327	0.00655	0.00367	0.00017		392	23	6	24	1
30c	23.4	332.7	0.07	0.04609	0.00878	0.02381	0.00448	0.00375	0.00013	2	283	24	4	24.1	0.8
31r	45.1	1321.5	0.03	0.04201	0.00421	0.01719	0.0017	0.00297	0.00007	-177	151	17	2	19.1	0.4
32c	6.3	175.9	0.04	0.04548	0.01927	0.02398	0.01008	0.00382	0.00022	-30	597	24	10	25	1
33r	74.3	1687.1	0.04	0.04762	0.0045	0.01941	0.00181	0.00296	0.00008	80	156	20	2	19.1	0.5
T604 amphibolitised granulite															
1	16.5	199.5	0.08	0.08031	0.02349	0.02911	0.00829	0.00263	0.00018	1205	495	29	8	17	1
2	12.2	329.4	0.04	0.0687	0.01312	0.02511	0.00469	0.00265	0.00012	890	325	25	5	17.1	0.8
3	15.3	448.4	0.03	0.04707	0.00832	0.01814	0.00315	0.00279	0.0001	53	267	18	3	18	0.6
4	8.9	146.7	0.06	0.04665	0.0181	0.01694	0.00651	0.00263	0.00014	31	550	17	7	16.9	0.9
5	13.7	182.6	0.08	0.06596	0.02382	0.02392	0.00848	0.00263	0.00019	805	594	24	8	17	1
6	20.7	263.1	0.08	0.07521	0.03612	0.02734	0.01282	0.00264	0.00028	1074	803	27	13	17	2
7	23.8	289.2	0.08	0.04899	0.01242	0.01847	0.00462	0.00273	0.00012	147	379	19	5	17.6	0.8
8	7.3	103.0	0.07	0.04725	0.03618	0.0158	0.012	0.00243	0.00024	62	1021	16	12	16	2
9	11.6	314.9	0.04	0.0467	0.01278	0.01728	0.00467	0.00268	0.00012	34	384	17	5	17.3	0.8
10	17.8	230.2	0.08	0.04438	0.01924	0.01612	0.00692	0.00263	0.00016	-51	593	16	7	17	1
11	17.1	319.4	0.05	0.06165	0.01378	0.02195	0.00483	0.00258	0.00011	662	408	22	5	16.6	0.7
12	9.1	184.8	0.05	0.04159	0.01882	0.01508	0.00679	0.00263	0.00013	-200	628	15	7	16.9	0.8
13	22.0	384.1	0.06	0.04608	0.01085	0.01703	0.00398	0.00268	0.00009	2	345	17	4	17.3	0.6
14	29.6	389.0	0.08	0.06926	0.01705	0.02598	0.00622	0.00272	0.00016	906	417	26	6	18	1
15	25.2	241.5	0.10	0.03265	0.01616	0.01143	0.00563	0.00254	0.00013	-170	602	12	6	16.4	0.8
16	22.6	317.2	0.07	0.04671	0.01557	0.01569	0.00518	0.00244	0.00012	34	471	16	5	15.7	0.8
17	19.3	355.1	0.05	0.04701	0.01173	0.01704	0.00418	0.00263	0.00013	50	348	17	4	16.9	0.8
18	15.3	178.7	0.09	0.06969	0.02513	0.02481	0.00878	0.00258	0.00018	919	609	25	9	17	1
19	12.7	195.3	0.07	0.04363	0.01951	0.01496	0.00664	0.00249	0.00015	-90	615	15	7	16	1
20	17.3	312.5	0.06	0.04838	0.01274	0.01769	0.00459	0.00265	0.00013	118	380	18	5	17.1	0.8
21	20.6	284.2	0.07	0.05136	0.01464	0.01777	0.00501	0.00251	0.00011	257	442	18	5	16.2	0.7
22	4.7	67.4	0.07	0.04663	0.04475	0.01637	0.01564	0.00255	0.00024	30	1128	16	16	16	2
T609 orthogneiss															
1r	3.8	200.1	0.02	0.05352	0.00555	0.02788	0.00283	0.00378	0.0001	351	181	28	3	24.3	0.6

757

2c	271.3	472.3	0.57	0.05735	0.00113	0.62788	0.01274	0.07941	0.0013	505	20	495	8	493	8
3r	4.5	352.7	0.01	0.05152	0.00348	0.02717	0.0018	0.00382	0.00008	264	113	27	2	24.6	0.5
4c	843.8	3525.4	0.24	0.05726	0.00101	0.62386	0.01147	0.07902	0.00128	502	18	492	7	490	8
5c	89.5	394.6	0.23	0.05784	0.00123	0.62961	0.01361	0.07895	0.0013	524	22	496	8	490	8
6c	361.6	915.6	0.39	0.05707	0.00111	0.62019	0.01239	0.07882	0.00129	494	20	490	8	489	8
7c	892.1	1118.3	0.80	0.05678	0.00105	0.6219	0.01193	0.07944	0.00129	483	19	491	7	493	8
8r	8.9	241.4	0.04	0.04742	0.00457	0.02486	0.00235	0.0038	0.00009	70	165	25	2	24.4	0.6
9c	59.0	202.1	0.29	0.0574	0.00246	0.62495	0.02635	0.07897	0.00148	507	60	493	16	490	9
10c	365.2	1862.0	0.20	0.05657	0.00118	0.61717	0.0131	0.07912	0.0013	475	22	488	8	491	8
11c	128.7	315.2	0.41	0.0583	0.00128	0.63221	0.01414	0.07865	0.0013	541	23	497	9	488	8
12c	515.2	2799.7	0.18	0.05627	0.00149	0.61564	0.01633	0.07936	0.00134	463	31	487	10	492	8
13r	3.6	185.8	0.02	0.05356	0.00648	0.02828	0.00335	0.00383	0.00011	353	214	28	3	24.6	0.7
14c	169.1	302.7	0.56	0.06647	0.00134	1.21732	0.02508	0.13282	0.00218	821	20	809	11	804	12
15c	123.7	292.4	0.42	0.05706	0.00138	0.62438	0.01523	0.07936	0.00132	494	27	493	10	492	8
16c	69.5	257.8	0.27	0.05741	0.00232	0.62025	0.02274	0.07836	0.00134	507	91	490	14	486	8
17c	621.7	3148.6	0.20	0.05667	0.00114	0.61745	0.01268	0.07902	0.00129	479	21	488	8	490	8
18r	12.9	294.2	0.04	0.04928	0.01096	0.02578	0.00561	0.00379	0.00019	161	325	26	6	24	1
19c	73.5	171.2	0.43	0.05676	0.0014	0.61868	0.01537	0.07905	0.00132	482	28	489	10	490	8
20c	185.5	575.4	0.32	0.05749	0.0015	0.62248	0.01622	0.07853	0.00132	510	30	491	10	487	8
21r	7.3	202.4	0.04	0.05456	0.00801	0.02841	0.00408	0.00378	0.00013	394	260	28	4	24.3	0.8
22c	300.9	888.8	0.34	0.08114	0.00267	2.08407	0.05905	0.18628	0.00311	1225	66	1144	19	1101	17
23r	5.2	274.5	0.02	0.04805	0.00381	0.02534	0.00197	0.00382	0.00009	102	129	25	2	24.6	0.6
24r	4.6	163.5	0.03	0.05255	0.00642	0.02595	0.00308	0.00358	0.0001	310	276	26	3	23	0.7
25c	51.9	179.8	0.29	0.05637	0.00181	0.61589	0.01957	0.07924	0.00138	467	40	487	12	492	8
26c	459.0	1155.9	0.40	0.05736	0.00135	0.62775	0.01481	0.07938	0.00132	505	25	495	9	492	8
27r	2.9	278.9	0.01	0.05106	0.00448	0.02646	0.00224	0.00376	0.00009	244	201	27	2	24.2	0.6
28c	368.5	498.8	0.74	0.05776	0.00144	0.63508	0.015	0.07974	0.00115	521	28	499	9	495	7
29c	277.8	598.5	0.46	0.05692	0.0018	0.61668	0.01864	0.07857	0.0012	488	40	488	12	488	7
30c	285.4	591.8	0.48	0.05738	0.00176	0.62097	0.01826	0.07849	0.00119	506	38	490	11	487	7
31c	91.5	344.2	0.27	0.05756	0.00168	0.6335	0.01764	0.07982	0.0012	513	35	498	11	495	7
32r	13.4	266.9	0.05	0.04605	0.00996	0.0227	0.00479	0.00358	0.00017		359	23	5	23	1

758

33c	149.3	238.4	0.63	0.05845	0.00193	0.62525	0.01978	0.07759	0.00121	547	42	493	12	482	7
34r	5.1	211.8	0.02	0.06785	0.0173	0.03407	0.00844	0.00364	0.00022	864	436	34	8	23	1
35c	1166.7	4479.5	0.26	0.05786	0.00165	0.62907	0.01721	0.07886	0.0012	524	34	496	11	489	7
36r	13.0	281.4	0.05	0.04686	0.00715	0.01708	0.00256	0.00264	0.00008	42	278	17	3	17	0.5
37c	205.2	500.9	0.41	0.0595	0.00208	0.63286	0.0214	0.07714	0.00124	585	46	498	13	479	7
T602 high-grade metasedimentary rock															
1r	9.3	724.1	0.01	0.06156	0.00116	0.7293	0.01129	0.08592	0.00092	659	41	556	7	531	5
2c	142.7	715.8	0.20	0.0713	0.00157	1.30223	0.02477	0.13247	0.00147	966	46	847	11	802	8
3r	41.3	3138.0	0.01	0.08548	0.00137	2.03718	0.0327	0.17285	0.00192	1326	15	1128	11	1028	11
4r	189.5	867.4	0.22	0.0671	0.00154	1.00399	0.02017	0.10851	0.0012	841	49	706	10	664	7
5c	550.2	497.4	1.11	0.07775	0.00124	1.81894	0.02918	0.16968	0.00189	1140	16	1052	11	1010	10
6c	315.3	464.9	0.68	0.07546	0.00129	1.86246	0.03177	0.17901	0.00201	1081	17	1068	11	1062	11
7c	93.0	110.7	0.84	0.07603	0.00283	1.79796	0.06541	0.17151	0.00252	1096	49	1045	24	1020	14
8c	310.6	546.5	0.57	0.07615	0.00128	1.94093	0.03275	0.18485	0.00207	1099	17	1095	11	1093	11
9c	159.3	362.2	0.44	0.07799	0.00134	1.81768	0.03122	0.16903	0.0019	1147	17	1052	11	1007	10
10c	102.8	178.7	0.57	0.1267	0.00283	6.50498	0.14329	0.37235	0.00471	2053	22	2047	19	2040	22
11c	210.6	305.4	0.69	0.07554	0.00257	1.80273	0.05726	0.17309	0.0021	1083	70	1046	21	1029	12
12c	168.8	270.5	0.62	0.0758	0.00139	1.90166	0.0347	0.18195	0.00208	1090	19	1082	12	1078	11
13r	1703.8	1580.1	1.08	0.05767	0.00105	0.61405	0.01119	0.07723	0.00088	517	21	486	7	480	5
14r	1666.2	1366.2	1.22	0.05849	0.00107	0.64434	0.01171	0.07989	0.00091	548	21	505	7	495	5
15c	144.2	354.3	0.41	0.11406	0.00209	5.07445	0.09291	0.32267	0.0037	1865	17	1832	16	1803	18
16r	192.5	1164.1	0.17	0.06727	0.00128	0.92022	0.01739	0.09921	0.00114	846	21	662	9	610	7
17r	12.4	966.9	0.01	0.07102	0.00153	1.06383	0.01953	0.10864	0.00122	958	45	736	10	665	7
18c	373.3	1325.9	0.28	0.06997	0.00191	1.33137	0.03277	0.13801	0.00161	927	57	859	14	833	9
19c	344.0	1121.6	0.31	0.0706	0.002	1.44052	0.03704	0.14799	0.00175	946	59	906	15	890	10
20r	99.0	496.5	0.20	0.07365	0.00162	1.07845	0.02346	0.1062	0.00127	1032	25	743	11	651	7
21c	60.8	718.2	0.08	0.06021	0.00165	0.78943	0.01961	0.09508	0.00111	611	61	591	11	586	7
22c	504.3	2328.5	0.22	0.09048	0.00193	2.96345	0.06273	0.23754	0.00282	1436	23	1398	16	1374	15
23c	97.3	175.6	0.55	0.09009	0.00202	2.88379	0.06395	0.23216	0.0028	1427	24	1378	17	1346	15
24c	89.9	685.4	0.13	0.07091	0.0019	1.332	0.03204	0.13625	0.00162	955	56	860	14	823	9
25c	178.5	302.1	0.59	0.0733	0.00158	1.52578	0.03231	0.15097	0.00177	1022	24	941	13	906	10
26c	71.4	206.1	0.35	0.07331	0.0019	1.70363	0.04342	0.16854	0.0021	1023	32	1010	16	1004	12
27c	356.6	943.0	0.38	0.08299	0.00187	2.29262	0.05099	0.20037	0.00239	1269	25	1210	16	1177	13
28r	3.2	257.7	0.01	0.05675	0.00865	0.02921	0.00438	0.00373	0.0001	482	345	29	4	24	0.7
29c	54.2	543.0	0.10	0.06982	0.00202	1.32124	0.03462	0.13724	0.00166	923	61	855	15	829	9
30c	115.3	244.0	0.47	0.06558	0.00199	1.14874	0.03428	0.12705	0.00167	793	41	777	16	771	10
31r	10.0	791.7	0.01	0.06071	0.00196	0.66868	0.0198	0.07988	0.00103	629	71	520	12	495	6
32c	245.6	287.5	0.85	0.10449	0.00288	4.13172	0.11258	0.28685	0.00374	1705	31	1661	22	1626	19
33r	5.5	299.9	0.02	0.07102	0.00253	1.07639	0.03769	0.10994	0.00156	958	48	742	18	672	9
34c	49.3	269.3	0.18	0.07082	0.00263	1.50452	0.05501	0.1541	0.00225	952	51	932	22	924	13
35r	9.4	738.3	0.01	0.07667	0.00239	1.43007	0.04067	0.13529	0.00175	1113	64	902	17	818	10
36c	161.6	960.6	0.17	0.06514	0.00272	1.16949	0.04609	0.13021	0.00179	779	90	786	22	789	10
37c	61.8	672.1	0.09	0.07497	0.00256	1.59396	0.05405	0.1542	0.00218	1068	45	968	21	924	12

Abbreviations: c, core; r, rim

Table 2. Trace elements data obtained by LA-ICP-MS for the granulites in the eastern Himalayan syntaxis.

Analysis	Hf	La	Ce	Pr	Nd	Sm	Eu	Gd	Tb	Dy	Ho	Er	Tm	Yb	Lu	Eu/Eu*	Ce/Ce*	$(Yb/Gd)_N$
T605 weakly retrograde granulite																		
1r	11776	0.01	1.72	0.01	0.39	1.49	0.73	7.62	1.88	15.38	4.42	16.26	3.14	29.69	5.51	0.54	71.1	4.8
2c	7890	0.01	2.48	0.01	0.48	1.16	1.00	5.31	1.54	14.57	4.55	18.45	3.51	34.29	6.55	1.03	66.8	8.0
3c	8476	0.01	0.57	0.01	0.10	0.29	0.17	1.69	0.57	5.55	1.61	5.81	1.05	8.77	1.45	0.56	11.1	6.4
4r	11610	0.01	2.16	0.02	0.52	1.75	0.66	8.56	2.37	17.93	4.36	12.90	2.16	17.04	2.77	0.42	30.2	2.5
5c	8010	0.00	2.11	0.01	0.36	0.97	0.80	4.72	1.26	10.76	3.20	12.53	2.53	23.04	4.52	0.94	44.6	6.0
6c	7553	0.01	2.87	0.03	0.54	1.29	1.13	6.17	1.85	17.48	5.65	22.68	4.64	41.99	7.92	1.01	22.8	8.4
7c	8071	0.01	1.80	0.02	0.30	0.72	0.66	4.17	1.14	12.01	3.99	16.44	3.35	32.84	6.30	0.91	24.7	9.8
8c	7824	0.01	1.94	0.01	0.29	0.71	0.52	3.60	1.02	10.59	3.60	15.38	3.24	30.53	5.89	0.80	51.4	10.5
9c	7135	0.01	2.31	0.02	0.22	0.66	0.65	3.83	1.18	11.00	3.47	13.29	2.65	25.25	4.50	0.97	36.5	8.2
10c	8056	0.01	1.23	0.01	0.06	0.19	0.16	0.94	0.30	3.31	1.07	4.51	1.05	9.23	1.67	0.96	42.7	12.2
11c	9613	0.01	0.37	0.00	0.02	0.05	0.08	0.78	0.26	2.76	0.79	2.96	0.51	4.71	0.74	0.71	14.8	7.5
12c	8937	0.01	0.79	0.01	0.14	0.34	0.32	2.22	0.74	6.88	2.19	8.16	1.77	17.05	3.21	0.85	27.4	9.5
13c	9600	0.01	0.67	0.01	0.03	0.10	0.11	1.10	0.32	2.92	0.69	2.35	0.39	3.05	0.47	0.66	19.5	3.4

14c	7500	0.00	2.15	0.02	0.18	0.64	0.44	2.91	0.89	8.87	2.90	11.17	2.14	20.01	3.64	0.82	37.4	8.5
15c	7945	0.01	1.51	0.01	0.19	0.25	0.29	2.01	0.60	5.95	2.13	8.25	1.74	17.53	3.11	0.89	43.6	10.8
16r	10683	0.00	2.50	0.01	0.17	1.14	0.43	6.40	1.71	13.98	3.69	12.32	2.16	17.33	2.64	0.39	90.9	3.4
17c	7932	0.01	1.92	0.02	0.32	1.03	0.66	4.15	1.27	11.95	3.86	15.69	3.27	30.32	5.68	0.84	27.8	9.1
18c	9114	0.01	0.79	0.01	0.19	0.26	0.22	1.19	0.45	4.02	1.12	3.80	0.70	6.61	1.10	1.02	23.8	6.9
19r	12261	0.01	2.40	0.04	0.97	3.88	1.44	15.3	3.56	23.55	4.92	13.38	2.01	14.34	2.10	0.49	15.9	1.2
20c	7863	0.02	2.33	0.01	0.17	0.46	0.33	2.34	0.66	6.82	2.06	7.82	1.63	14.80	2.62	0.79	42.8	7.9
21c	8410	0.01	1.76	0.01	0.09	0.24	0.25	1.44	0.52	4.79	1.49	6.14	1.21	10.45	1.81	0.99	57.6	9.0
22c	9560	0.01	0.34	0.01	0.10	0.29	0.28	1.47	0.51	4.68	1.23	4.23	0.81	6.91	1.13	1.06	9.0	5.8
23c	7482	0.01	2.39	0.01	0.13	0.52	0.44	2.70	0.73	6.80	2.11	7.95	1.63	14.74	2.76	0.92	63.0	6.8
24r	12288	0.01	1.84	0.01	0.36	1.41	0.63	8.91	2.28	16.91	3.81	11.10	1.85	13.42	2.17	0.41	36.9	1.9
25c	7739	0.01	2.29	0.02	0.36	0.99	0.77	4.43	1.22	11.09	3.38	13.66	2.57	24.93	4.81	0.94	33.7	7.0
26c	7861	0.01	1.71	0.01	0.06	0.35	0.31	1.67	0.57	6.41	2.38	10.01	2.14	20.69	4.09	1.03	50.5	15.4
27r	10237	0.01	1.48	0.02	0.40	1.40	0.63	6.45	1.69	14.43	4.04	15.13	2.91	27.49	5.24	0.53	16.1	5.3
28c	6791	0.01	2.00	0.01	0.33	0.94	0.57	3.50	0.95	8.69	2.67	9.74	1.84	18.18	3.35	0.84	37.3	6.4
29c	7729	0.01	1.73	0.01	0.14	0.35	0.53	2.79	0.90	9.66	3.25	14.53	2.93	28.43	6.05	1.16	41.9	12.6
30c	7781	0.01	1.92	0.02	0.46	1.12	0.79	4.64	1.33	12.74	3.93	16.01	3.07	29.49	5.68	0.91	25.3	7.9
31r	11997	0.01	1.80	0.01	0.30	1.44	0.52	6.99	1.79	11.80	2.49	6.70	0.97	7.05	1.03	0.41	33.3	1.2
32c	8546	0.01	0.93	0.01	0.07	0.23	0.11	0.85	0.23	2.14	0.72	3.10	0.59	5.42	1.05	0.65	27.5	7.9
33r	10532	0.01	1.59	0.04	0.48	1.35	0.54	6.10	1.42	9.73	2.28	7.04	1.10	9.35	1.49	0.48	12.1	1.9
T604 amphibolitised granulite																		
1	8774	0.01	1.30	0.01	0.06	0.24	0.21	1.70	0.96	12.91	6.31	34.65	8.94	105.63	24.76	0.73	31.9	77.0
2	10509	0.03	1.34	0.01	0.18	0.39	0.29	3.02	1.37	19.54	8.34	45.10	11.34	130.74	29.18	0.57	18.8	53.6
3	10470	0.01	1.43	0.00	0.03	0.21	0.17	2.52	1.01	14.90	6.45	34.26	8.39	95.65	21.97	0.42	67.1	47.0
4	8599	0.01	0.87	0.01	0.07	0.12	0.10	0.85	0.43	6.62	2.95	15.65	3.94	46.11	10.99	0.72	29.9	67.5
5	8778	0.01	1.22	0.01	0.06	0.09	0.14	1.68	0.71	10.43	4.77	27.40	7.18	86.12	21.34	0.54	30.4	63.5
6	8312	0.01	1.71	0.01	0.13	0.12	0.10	1.19	0.68	8.76	4.16	23.44	5.99	67.39	16.56	0.50	36.4	70.2
7	8766	0.01	1.67	0.01	0.14	0.48	0.25	3.35	1.48	21.24	9.64	48.54	11.84	135.29	31.97	0.44	72.0	50.0
8	9911	0.00	0.76	0.01	0.06	0.09	0.10	1.06	0.56	8.14	3.82	20.99	5.03	58.87	13.64	0.59	26.2	68.8
9	10341	0.01	1.18	0.01	0.07	0.20	0.13	1.41	0.73	10.54	4.98	26.21	6.60	80.35	18.32	0.54	47.2	70.9
10	8521	0.01	1.31	0.01	0.08	0.23	0.26	1.83	0.88	12.44	5.95	31.73	7.84	93.58	22.41	0.87	40.9	63.4

761

11	10111	0.00	1.22	0.01	0.09	0.34	0.13	2.41	1.01	15.81	7.11	38.67	9.93	116.55	27.63	0.32	49.1	59.9
12	9709	0.01	0.84	0.01	0.10	0.21	0.11	1.57	0.73	10.57	4.72	25.98	6.58	77.20	18.22	0.40	20.9	61.1
13	9749	0.01	1.61	0.01	0.06	0.29	0.30	2.70	1.24	18.32	8.26	43.99	11.12	130.60	30.15	0.68	42.3	59.9
14	8347	0.01	2.00	0.01	0.08	0.33	0.33	2.17	1.18	17.32	7.91	41.70	9.93	113.02	25.22	0.89	54.7	64.5
15	8897	0.01	1.39	0.00	0.07	0.32	0.31	2.85	1.34	17.84	7.89	40.37	9.92	115.13	26.46	0.66	48.0	50.1
16	9033	0.01	1.64	0.01	0.07	0.37	0.28	3.65	1.54	21.99	10.15	55.05	14.04	168.27	40.24	0.48	42.2	57.1
17	9936	0.01	1.51	0.01	0.15	0.37	0.22	3.14	1.60	21.82	10.30	55.49	14.17	163.30	39.22	0.43	41.3	64.4
18	8137	0.01	1.11	0.01	0.07	0.08	0.15	1.74	0.70	10.59	4.97	27.35	6.57	78.76	18.92	0.57	30.4	56.1
19	9686	0.01	1.11	0.01	0.07	0.12	0.20	1.91	0.90	13.41	6.25	33.39	8.60	105.75	25.04	0.69	35.3	68.6
20	10234	0.01	1.44	0.00	0.13	0.21	0.20	2.80	1.18	18.10	8.63	46.48	11.97	143.44	34.65	0.45	65.7	63.5
21	8756	0.01	1.51	0.01	0.12	0.36	0.28	3.10	1.34	19.83	9.01	48.78	12.51	149.47	35.77	0.55	39.8	59.8
22	9040	0.01	0.63	0.01	0.06	0.13	0.10	1.42	0.56	8.60	3.92	21.23	5.33	61.32	14.82	0.46	19.4	53.6

Abbreviations: c, core; r, rim. The subscript 'N' denotes that the concentration is normalized to chondrite.

762